NAVAL POSTGRADUATE SCHOOL

MONTEREY, CALIFORNIA

THESIS

OPTIMAL DESIGN OF PIEZOELECTRIC MATERIALS FOR MAXIMAL ENERGY HARVESTING

by

Russell J. Nelson

June 2015

Thesis Advisor: Hong Zhou
Second Reader: Susan M. Sanchez

THIS PAGE INTENTIONALLY LEFT BLANK

REPORT DOCUMENTATION PAGE

Form Approved OMB No. 0704–0188

1. AGENCY USE ONLY *(Leave Blank)*	2. REPORT DATE	3. REPORT TYPE AND DATES COVERED
	06-19-2015	Master's Thesis 11-01-2013 to 06-19-2015

4. TITLE AND SUBTITLE

OPTIMAL DESIGN OF PIEZOELECTRIC MATERIALS FOR MAXIMAL ENERGY HARVESTING

5. FUNDING NUMBERS

6. AUTHOR(S)

Russell J. Nelson

7. PERFORMING ORGANIZATION NAME(S) AND ADDRESS(ES)

Naval Postgraduate School
Monterey, CA 93943

8. PERFORMING ORGANIZATION REPORT NUMBER

9. SPONSORING / MONITORING AGENCY NAME(S) AND ADDRESS(ES)

N/A

10. SPONSORING / MONITORING AGENCY REPORT NUMBER

11. SUPPLEMENTARY NOTES

The views expressed in this document are those of the author and do not reflect the official policy or position of the Department of Defense or the U.S. Government. IRB Protocol Number: N/A.

12a. DISTRIBUTION / AVAILABILITY STATEMENT

Approved for public release; distribution is unlimited

12b. DISTRIBUTION CODE

13. ABSTRACT *(maximum 200 words)*

The military's dependence on fossil fuels for electric power production in isolated settings is both logistically and monetarily expensive. Currently, the Department of Defense is actively seeking alternative methods to produce electricity, thus decreasing dependence on fossil fuels and increasing combat power. We believe piezoelectric generators have the ability to contribute to military applications of alternative electrical power generation in isolated and austere conditions. In this paper, we use three and six variable mathematical models to analyze piezoelectric generator power generation capabilities. Using m^k factorial sampling, nearly orthogonal and balanced Latin hypercube (NOBLH) design, and NOBLH iterative methods, we find optimal solutions to maximize piezoelectric generator power output. We further analyze our optimal results using robustness analysis techniques to determine the sensitivity of our models to variable precision. With our results, we provide analysts and engineers the optimal designs involving material parameters in the piezoelectric generator, as well as the generator's environment, in order to maximize electric output.

14. SUBJECT TERMS	15. NUMBER OF PAGES
piezoelectric power optimization, nearly orthogonal and balanced Latin hypercube design, factorial sampling, nearly orthogonal and balanced Latin hypercube design iterative method, robustness analysis	115
	16. PRICE CODE

17. SECURITY CLASSIFICATION OF REPORT	18. SECURITY CLASSIFICATION OF THIS PAGE	19. SECURITY CLASSIFICATION OF ABSTRACT	20. LIMITATION OF ABSTRACT
Unclassified	Unclassified	Unclassified	UU

NSN 7540-01-280-5500

Standard Form 298 (Rev. 2–89)
Prescribed by ANSI Std. 239–18

THIS PAGE INTENTIONALLY LEFT BLANK

Approved for public release; distribution is unlimited

OPTIMAL DESIGN OF PIEZOELECTRIC MATERIALS FOR MAXIMAL ENERGY HARVESTING

Russell J. Nelson
Captain, United States Army
B.S., United States Military Academy, 2005

Submitted in partial fulfillment of the
requirements for the degree of

MASTER OF SCIENCE IN APPLIED MATHEMATICS

from the

NAVAL POSTGRADUATE SCHOOL
June 2015

Author: Russell J. Nelson

Approved by: Hong Zhou
Thesis Advisor

Susan M. Sanchez
Second Reader

Craig Rasmussen
Chair, Department of Applied Mathematics

THIS PAGE INTENTIONALLY LEFT BLANK

ABSTRACT

The military's dependence on fossil fuels for electric power production in isolated settings is both logistically and monetarily expensive. Currently, the Department of Defense is actively seeking alternative methods to produce electricity, thus decreasing dependence on fossil fuels and increasing combat power. We believe piezoelectric generators have the ability to contribute to military applications of alternative electrical power generation in isolated and austere conditions. In this paper, we use three and six variable mathematical models to analyze piezoelectric generator power generation capabilities. Using m^k factorial sampling, nearly orthogonal and balanced Latin hypercube (NOBLH) design, and NOBLH iterative methods, we find optimal solutions to maximize piezoelectric generator power output. We further analyze our optimal results using robustness analysis techniques to determine the sensitivity of our models to variable precision. With our results, we provide analysts and engineers the optimal designs involving material parameters in the piezoelectric generator, as well as the generator's environment, in order to maximize electric output.

THIS PAGE INTENTIONALLY LEFT BLANK

Table of Contents

List of Figures

List of Tables

Acknowledgments

The professionalism, expertise, and mentorship of the Naval Postgraduate School Applied Mathematics Department contributed greatly to my success at NPS. In particular, I would like to thank my thesis advisor, Dr. Hong Zhou, and second reader, Dr. Susan Sanchez. I learned a tremendous amount while working with these phenomenal professors.

My wife, Sarah, and two wonderful boys kept me grounded throughout my time at NPS, serving as a constant reminder of what is important in life. Thank you for supporting me and agreeing to go where the Army sends us. I am blessed to have you in my life.

Finally, I would be remiss not to thank the students from my cohort, Lieutenant Philip Baxa, Captain Benjamin Davis, and Captain Matthew Fletcher. We struggled through several tough quarters together. Thank you for your friendship.

THIS PAGE INTENTIONALLY LEFT BLANK

CHAPTER 1:
Introduction

1.1 Motivation

"Unleash us from the tether of fuel."

-Lieutenant General Jamis Mattis,
Future Fuels, Naval Research
Advisory Committee Report
April 2006

During the past decade of conflict, service members on bases across Iraq and Afghanistan could hear the constant hum of diesel generators. These thirsty machines provide the base's electric lifeblood enabling lighting, refrigeration, life-support heating and cooling, battery charging, and equipment operation. Years of conflict proved our dependence on fossil fuels comes with a cost. A constant consumption of diesel fuel requires a hefty logistics tail to provide fossil fuels to every base across the area of operations. During Operation Iraqi Freedom and Operation Enduring Freedom an Army study found that, for every 24 convoys sent out, one service member or civilian engaged in fuel transport was killed. Additionally, due to transportation cost of fossil fuels to isolated bases, the price of fuel escalates from approximately one dollar per gallon to, in some cases, 400 dollars per gallon [1].

The source of electricity generation service members depend on decreases combat capability. Military forces are taken away from combat operations and nation building to guard and operate convoys. Dollars spent on expensive fossil fuels are better allocated to support service members and operations. Additionally, expeditionary forces do not have the ability to transport heavy fuels. Their dependence on fossil fuels for power generation inhibits their ability to conduct operations.

This paper attempts to improve upon an alternative method of producing electricity while in austere conditions without the necessity of fossils fuels and their accompanying logistics tail.

Figure 1.1: Soldier guarding fuel convoy after attack [2].

1.2 Piezoelectricity Definition and History

The name "piezo" is derived from the Greek *piezo* or *piezein*, meaning "to squeeze or press" [3]. Piezoelectricity is pressure-driven electricity. Certain materials generate electricity when under pressure (mechanical stress). These same materials change shape when electricity is applied to the material. A common use of the piezoelectricity phenomenon is demonstrated in quartz watches. A battery in the watch feeds electricity to a piezoelectric quartz crystal. The electricity induces a precise vibration in the quartz. The mechanisms in the watch then convert the quartz vibrations into a means of keeping accurate time.

Figure 1.2: Piezoelectric quartz crystal resonator used for time keeping [4].

In 1880, two French physicists, Pierre and Jacques Curie, found that in certain materials, such as zinc blende, sodium chlorate, boracite, tourmaline, cane sugar, Rochelle salt, and quartz, mechanical stresses induce macroscopic polarization and hence the production of electric surface charges. The following year, Gabriel Lippmann predicted the converse effect from fundamental thermodynamic principles, that is, an imposed voltage produces mechanical deformations or strains of the material [5]. In 1882, the Curie brothers confirmed the existence of the converse effect based on experimental observations [3].

Pierre Curie used the piezoelectric effect to measure charges emitted by radium, but piezoelectricity was not used for practical applications for several decades. During World War I, Paul Langevin developed piezoelectric crystal quartz transducer depth sounding devices to locate submerged vessels, primarily German submarines [6]. In the 1920s, developments in crystal resonators for the stabilization of oscillators launched the field of frequency of control. The introduction of quartz control drastically changed the way humans keep time. Today, piezoelectric applications include smart materials for vibration control, aerospace and astronautical applications of flexible surfaces and structures, sensors for robotic applications, and novel applications for vibration reduction in sports equipment (tennis racquets

and snowboards) [5]. Recently, scientists have focused research on using piezoelectric materials for energy generation [7]–[14].

1.3 How Piezoelectricity Works

The separation of positive and negative electrical charges in many molecules results in what is known as a dipole moment. In piezoelectric crystals, when a mechanical stress is applied (the crystal being compressed, twisted, or pulled) the molecular dipole moments re-orient themselves. This re-orientation causes a variation in surface charge density and thus produces voltage. The effect is illustrated in Figure 1.3 for forces normal to the material. Conversely, when an electric field is applied across a piezoelectric medium, there is a slight change in the shape of the dipoles causing a very small, but significant change in the material dimensions.

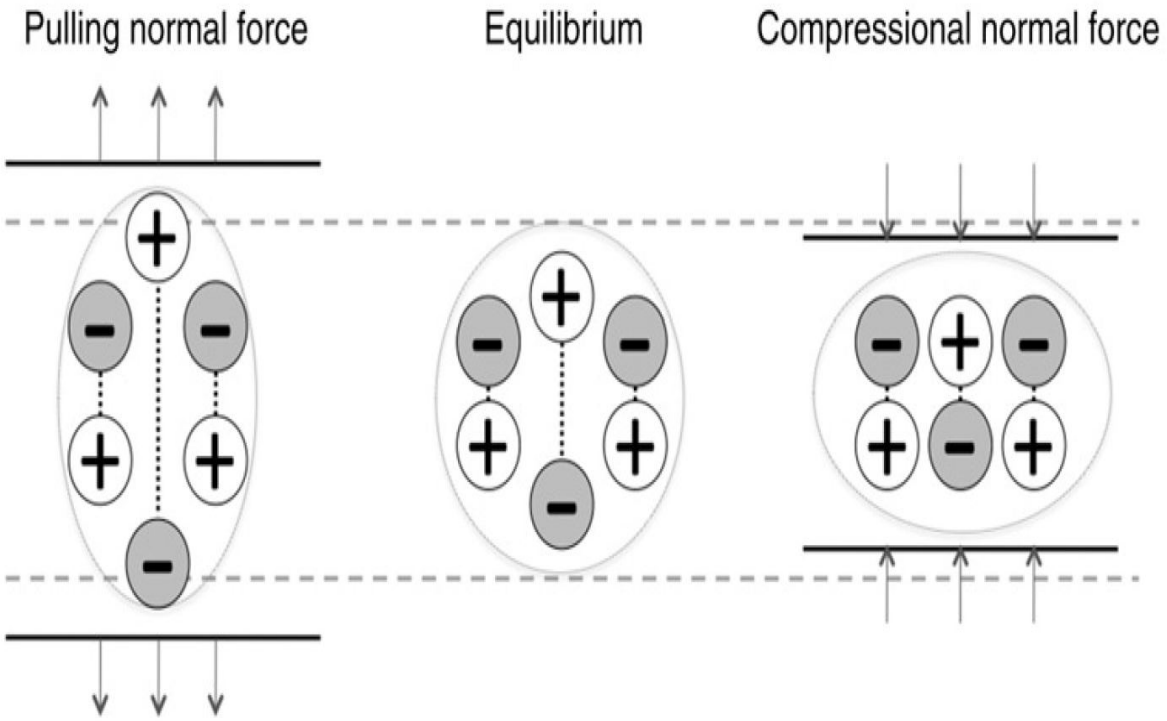

Figure 1.3: Illustration of the piezoelectric concept [3].

1.4 Applications of Piezoelectric Power Generation

Using the converse piezoelectric effect, it is possible to generate electricity by deforming piezoelectric materials. However, piezoelectric generation is far from the most efficient method of power generation. Presently, piezoelectric generators can only produce small amounts of electricity, but with the increase of efficiency of powered devices, piezoelectric power generation has become a possible supply of electricity for certain devices.

Devices well suited for piezoelectric power supply include the following:

- devices with low power requirements
- devices without power supplies in close proximity
- devices without easy access to a power supply (power lines are inconvenient or impossible)
- devices without access to other alternative power sources (solar, wind, geothermal)
- devices with access to vibrations or other mechanical manipulation

The most obvious device that meets the above criteria is a sensor. Sensors are often located far from power sources, concealed from light sources, and require power to collect and send information. It is not always possible or convenient to connect power to the sensors by wire. Examples of sensors that could receive power through piezoelectric generation include sensors in air ducts [15], tires, and inside machinery.

Piezoelectric power generation has the potential to enhance military operations as well. Military units often operate in primitive/isolated environments where it is not practical to transport conventional fuel to generate electricity. Military units must rely on alternative methods of power generation or do without. In addition to solar and wind power generation, service members could generate power with piezoelectric power generators fixed to personnel, equipment, or any other item in motion.

1.5 Research Objectives

This paper attempts to find the optimal designs involving material parameters in the piezoelectric generator, as well as the generator's environment, in order to maximize electric output.

1.6 Thesis Organization

This chapter introduced the motivation and relevant background of harvesting piezoelectric energy. In Chapter 2, we review a one-dimensional power generation model and study how to optimize power generation using variables in the model. From the results of Chapter 2 we derive a three-variable power generation model. In Chapter 3, we derive a six-variable power generation model using a single mode model. In Chapter 4, we describe the various methods we use in order to optimize our three-variable and six-variable power generation models. In Chapter 5, we discuss the results of our optimization methods and the robustness of our results. In Chapter 6, we conclude the paper and discuss further studies to be completed based on the information and ideas generated in this paper. Finally, we include an appendix to display MATLAB code used for calculations within the paper.

CHAPTER 2:
One-Dimensional Power Generation Model:
Derivation of the Three Variable Model

2.1 1-D Model Design: Interpretation Scheme

We can use a basic 1-D model to analyze the power generated from a vibration energy harvester to understand conversion. This model is limited to harvesters where the electrical damping term is linear and proportional to velocity. Nevertheless, this simple model is useful in understanding the feasibility of the device and input parameters on power extracted. The electrical energy is extracted from the mechanical system, which is excited by a mechanical input. This extraction is not necessarily linear, or proportional to velocity, however, it is a dissipative process and can generally be viewed as electrical damping.

Following [16], we consider a generator (shown in Figure 2.1) which consists of a seismic mass m on a spring k. When the generator is vibrated, the mass moves out of phase with the generator housing, so that there is a net movement between the mass and the housing. This relative displacement is sinusoidal in amplitude, and can drive a suitable transducer to generate electrical energy. The transducer is depicted as a dashpot, d, because the conversion of mechanical energy into electrical energy damps the mass. There are several transduction methods suitable for the generator. The choice of transducer makes little difference to the amount of electrical power that will be generated. Three possible transduction mechanisms are (1) piezoelectric: using piezoelectric material to convert strain in the spring into electricity; (2) electromagnetic: a magnet attached to the mass induces a voltage in a coil as it moves; and (3) electrostatic: an electric arrangement with a permanent charge embedded in the mass induces a voltage on the plates of a capacitor as it moves.

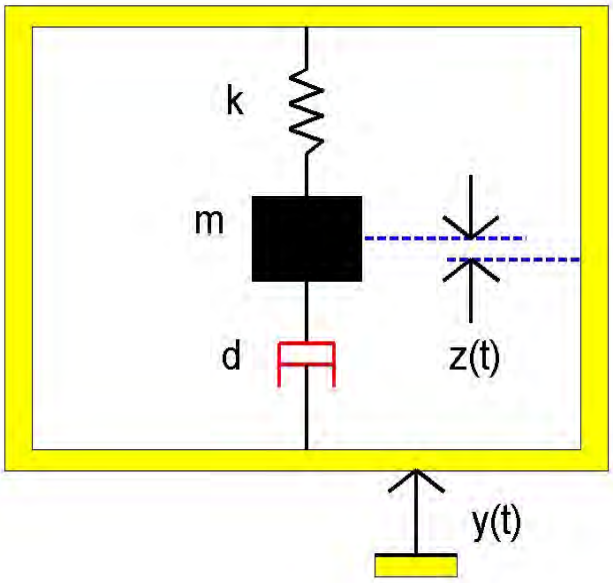

Figure 2.1: A schematic diagram of the generator [17].

In the simplified model, we assume that the mass of the vibration source is much bigger than the mass of the seismic mass in the generator, and the vibration source is an infinite source of power. This implies that the vibration source is unaffected by the movement of the generator.

The differential equation of motion can be derived from the dynamic forces on the mass:

$$mz''(t) + dz'(t) + kz(t) = -my''(t) \tag{2.1}$$

where the generator housing is vibrated with a displacement $y(t)$, the relative motion of the mass with respect to the housing is $z(t)$, m is the seismic mass, d is the damping constant,

and k is the spring constant. The solution to this second-order ordinary differential equation (ODE) with constant coefficients consists of two parts, the complementary function, which is the solution of the corresponding homogeneous equation, and the particular solution. The complementary function, in this case, is a damped free vibration which goes to zero as time increases. The particular solution is the one of interest here. For a sinusoidal excitational vibration, $y(t) = Y_0 cos(\omega t)$, the particular solution to the preceding ODE is a steady-state oscillation of the same frequency, ω, as that of the excitation. We can assume the particular solution to be of the form

$$z(t) = A cos(\omega t - \phi) \tag{2.2}$$

where A is the amplitude of oscillation and ϕ is the phase of the displacement with respect to the exciting force.

Differentiating Equation (2.2) yields

$$z'(t) = -A\omega \sin(\omega t - \phi), \tag{2.3}$$

$$z''(t) = -A\omega^2 \cos(\omega t - \phi). \tag{2.4}$$

Substituting the above equations into Equation (2.1) we have

$$-Am\omega^2 \cos(\omega t - \phi) - Ad\omega \sin(\omega t - \phi) + Ak \cos(\omega t - \phi) = mY_0\omega^2 \cos(\omega t). \tag{2.5}$$

Utilizing the trigonometric identities $cos(\omega t - \phi) = cos(\omega t)cos(\phi) + sin(\omega t)sin(\phi)$ and $sin(\omega t - \phi) = sin(\omega t)cos(\phi) - cos(\omega t)sin(\phi)$ we can rewrite Equation (2.5) as

$$\begin{aligned} -Am\omega^2 \cos\omega t \cos\phi - Am\omega^2 \sin\omega t \sin\phi - Ad\omega \sin\omega t \cos\phi + Ad\omega \cos\omega t \sin\phi \\ +Ak \cos\omega t \cos\phi + Ak \sin\omega t \sin\phi = mY_0\omega^2 \cos(\omega t). \end{aligned} \tag{2.6}$$

Matching the coefficients for $cos(\omega t)$ and $sin(\omega t)$, respectively, we find

$$\left(Ak - Am\omega^2\right) \cos\phi + Ad\omega \sin\phi = mY_0\omega^2, \tag{2.7}$$

$$\left(k - m\omega^2\right) \sin\phi - d\omega \cos\phi = 0. \tag{2.8}$$

This leads to

$$\tan\phi = \frac{d\omega}{k - m\omega^2}, \tag{2.9}$$

$$\left[\left(k - m\omega^2\right)\cos\phi + d\omega\sin\phi\right]A = mY_0\omega^2, \tag{2.10}$$

$$\left[\left(k - m\omega^2\right) + d\omega\tan\phi\right]A = mY_0\omega^2\sec\phi = mY_0\omega^2\sqrt{1+\tan^2\phi}. \tag{2.11}$$

Solving for A, we obtain

$$A = \frac{mY_0\omega^2\sqrt{1+\tan^2\phi}}{(k-m\omega^2)+d\omega\tan\phi} = \frac{mY_0\omega^2\sqrt{1+\left(\frac{d\omega}{k-m\omega^2}\right)^2}}{(k-m\omega^2)+d\omega\left(\frac{d\omega}{k-m\omega^2}\right)} = \frac{mY_0\omega^2\sqrt{\left(k-m\omega^2\right)^2+\left(d\omega\right)^2}}{\left(k-m\omega^2\right)^2+\left(d\omega\right)^2}, \tag{2.12}$$

$$A = \frac{mY_0\omega^2}{\sqrt{\left(k-m\omega^2\right)^2+\left(d\omega\right)^2}}. \tag{2.13}$$

We now express the amplitude and phase in non-dimensional form. Dividing the numerator and denominator by k, we get

$$\tan\phi = \frac{d\omega}{k-m\omega^2} = \frac{\frac{d\omega}{k}}{1-\frac{m\omega^2}{k}}, \tag{2.14}$$

$$A = \frac{Y_0\frac{m\omega^2}{k}}{\sqrt{\left(1-\frac{m\omega^2}{k}\right)^2+\left(\frac{d\omega}{k}\right)^2}}. \tag{2.15}$$

These expressions can be further expressed in terms of the following quantities where ω_n is the natural frequency of undamped oscillation (resonant angular frequency), d_c is critical damping, and ζ is the modal damping ratio:

$$\omega_n = \sqrt{\frac{k}{m}}, \tag{2.16}$$

$$d_c = 2m\omega_n, \tag{2.17}$$

$$\frac{d\omega}{k} = \frac{d}{d_c}\frac{d_c\omega}{k} = 2\zeta\frac{\omega}{\omega_n}, \tag{2.18}$$

$$\frac{k}{d_c} = \frac{k}{2m\omega_n} = \frac{k/m}{2\sqrt{\frac{k}{m}}} = \frac{1}{2}\sqrt{\frac{k}{m}} = \frac{\omega_n}{2}. \tag{2.19}$$

The non-dimensional formulas for the amplitude and phase then become

$$\tan\phi = \frac{2\zeta\frac{\omega}{\omega_n}}{1-\left(\frac{\omega}{\omega_n}\right)^2}, \tag{2.20}$$

$$\frac{A}{Y_0} = \frac{\left(\frac{\omega}{\omega_n}\right)^2}{\sqrt{\left(1-\frac{\omega^2}{\omega_n{}^2}\right)^2 + \left(2\zeta\frac{\omega}{\omega_n}\right)^2}}. \tag{2.21}$$

The instantaneous power transfer in the mass is the product of the force on the mass and its velocity:

$$p(t) = -my''(t)\left[y'(t) + z'(t)\right]. \tag{2.22}$$

When damping is present, due to the electrical transducer, there is a net transfer of mechanical power into electrical power. This net electrical power generated, P, is

$$P = \frac{1}{T}\int_0^T p(t)\,dt = \frac{1}{T}\int_0^T m\omega^2 Y_0\cos(\omega t)\left[-Y_0\omega\sin(\omega t) - A\omega\sin(\omega t-\phi)\right]dt, \tag{2.23}$$

$$P = \frac{1}{T}\int_0^T mA\omega^3 Y_0\sin\phi\cos^2(\omega t)dt = \frac{1}{T}\int_0^T mA\omega^3 Y_0\sin\phi\,\frac{1+\cos(2\omega t)}{2}dt, \tag{2.24}$$

$$P = mY_0\omega^3\frac{A}{2}\sin\phi. \tag{2.25}$$

Substituting in Equation (2.21) for A, we obtain:

$$P = mY_0{}^2\omega^3\frac{\left(\frac{\omega}{\omega_n}\right)^2}{2\sqrt{\left(1-\frac{\omega^2}{\omega_n{}^2}\right)^2 + \left(2\zeta\frac{\omega}{\omega_n}\right)^2}}\frac{1}{\sqrt{1+\cot^2\phi}}, \tag{2.26}$$

$$P = mY_0{}^2\omega^3 \frac{\left(\frac{\omega}{\omega_n}\right)^2}{2\sqrt{\left(1-\frac{\omega^2}{\omega_n{}^2}\right)^2+\left(2\zeta\frac{\omega}{\omega_n}\right)^2}} \frac{1}{\sqrt{1+\left[\frac{1-\left(\frac{\omega}{\omega_n}\right)^2}{2\zeta\frac{\omega}{\omega_n}}\right]^2}}, \tag{2.27}$$

$$P = \frac{mY_0{}^2\omega^3\left(\frac{\omega}{\omega_n}\right)^2\zeta\frac{\omega}{\omega_n}}{\left(1-\frac{\omega^2}{\omega_n{}^2}\right)^2+\left(2\zeta\frac{\omega}{\omega_n}\right)^2} = \frac{m\zeta Y_0{}^2\left(\frac{\omega}{\omega_n}\right)^3\omega^3}{\left(1-\frac{\omega^2}{\omega_n{}^2}\right)^2+\left(2\zeta\frac{\omega}{\omega_n}\right)^2}. \tag{2.28}$$

We now have an explicit expression for net electric power generated we can conduct analysis on. In the following sections we first view the output power as a function of normalized frequency and investigate how the output power behaves as we vary normalized frequency for various values of the modal damping ratio. After that, we treat the output power as a multi-variable function of both normalized frequency and modal damping ratio, seeking the optimal value of the output power. Then, we compare our model prediction with an experimental result.

2.2 Power as a Function of Normalized Frequency

First, we will treat net electric power generated, P, as a function of normalized frequency only. To do this, we will introduce $C = m\zeta Y_0^2\omega_n^3$ and $x = \frac{\omega}{\omega_n}$ to get the function

$$P(x) = C\frac{x^6}{(1-x^2)^2+(2\zeta x)^2}. \tag{2.29}$$

In order to optimize the function we differentiate $P(x)$ with respect to x:

$$P'(x) = \frac{2Cx^5\left[x^4-4x^2+8\zeta^2x^2+3\right]}{\left(x^4+4\zeta^2x^2-2x^2+1\right)^2}. \tag{2.30}$$

By inspection, we can see if $\zeta = 0$, $P'(x)$ does not exist when $x = 1$. In fact, P(1) becomes infinitely large. If $\zeta \neq 0$, the critical points of $P(x)$ depend on the value of ζ.

2.2.1 Initial Analysis

We will fix values for ζ and find the value of x that maximizes $P(x)$. Like Williams and Yates [17], we will analyze $P(x)$ with ζ values of $0.1, 0.3, 0.5$, and 0.7.

For $\zeta = 0.1$,

$$P'(x) = \frac{2Cx^5\left[x^4 - 3.92x^2 + 3\right]}{\left(x^4 - 1.96x^2 + 1\right)^2}. \tag{2.31}$$

Solving $P'(x) = 0$ yields critical points $x = \pm 1.6963, \pm 1.0211$. Recall that $x = \frac{\omega}{\omega_n} \geq 0$. For $\zeta = 0.1$, we plot $\frac{P(x)}{C}$ as a function of x in an interval containing the critical points in Figure 2.2.

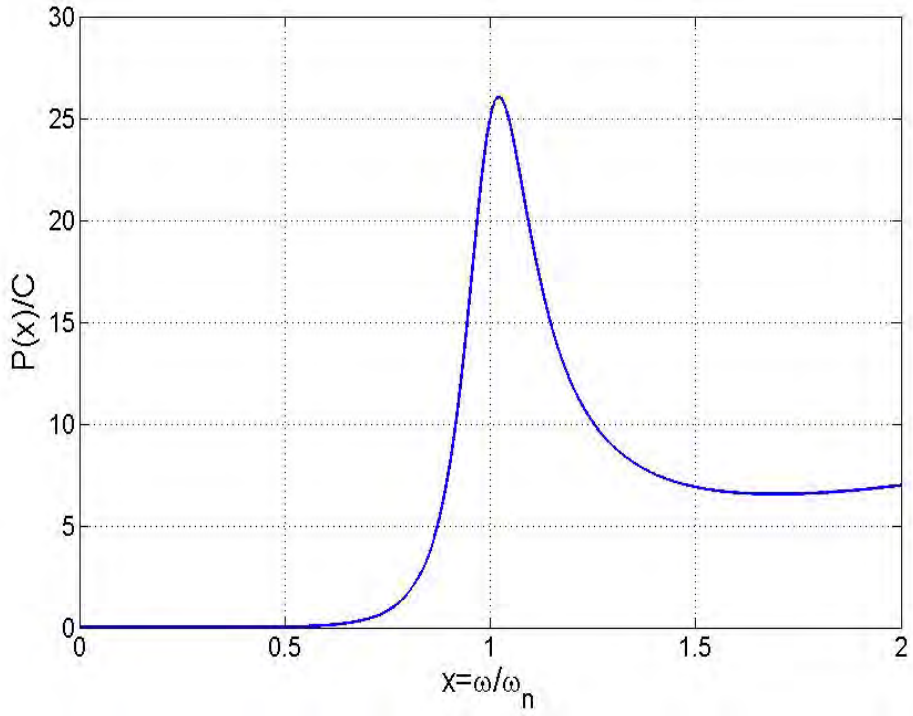

Figure 2.2: Power as a function of frequency with $\zeta = 0.1$.

From Figure 2.2, we can see that the maximum power can be generated when $x = \frac{\omega}{\omega_n} = 1.0211$ for $\zeta = 0.1$, and the maximum value of $\frac{P(x)}{C}$ is 26.0421.

For $\zeta = 0.3$,

$$P'(x) = \frac{2Cx^5\left[x^4 - 3.28x^2 + 3\right]}{\left(x^4 - 1.64x^2 + 1\right)^2}. \tag{2.32}$$

Solving $P'(x) = 0$ yields four complex roots. The critical point is $x = 0$. Now we plot $\frac{P(x)}{C}$ for $\zeta = 0.3$ in Figure 2.3.

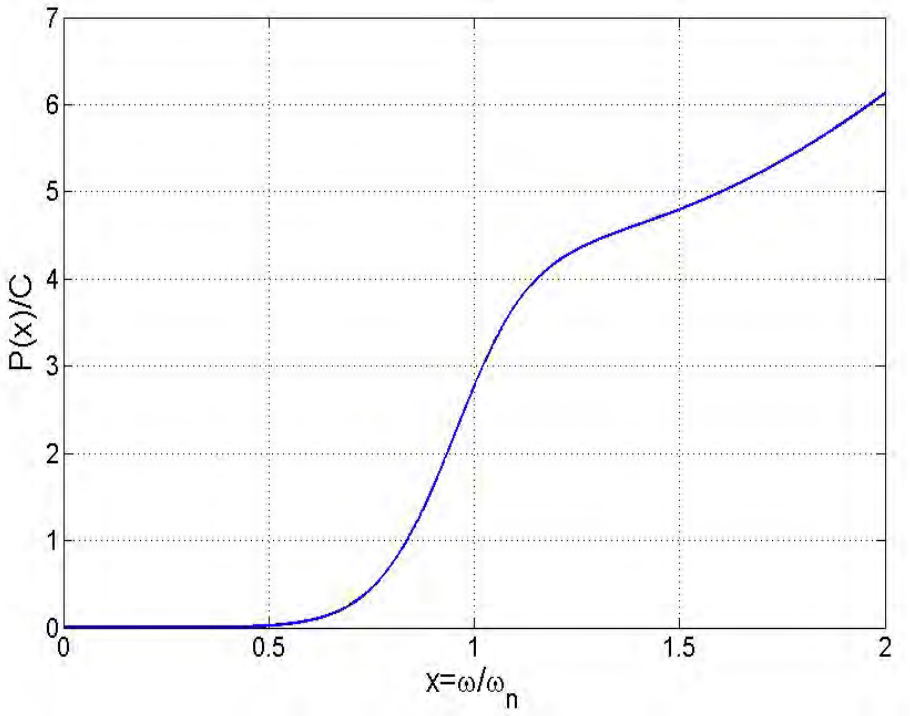

Figure 2.3: Power as a function of frequency with $\zeta = 0.3$.

Figure 2.3 shows when $\zeta = 0.3$, $\frac{P(x)}{C}$ is an increasing function of x.

For $\zeta = 0.5$,

$$P'(x) = \frac{2Cx^5\left[x^4 - 2x^2 + 3\right]}{\left(x^4 - x^2 + 1\right)^2}. \tag{2.33}$$

Solving $P'(x) = 0$ yields four complex roots. The critical point is $x = 0$. Now we plot $\frac{P(x)}{C}$ for $\zeta = 0.5$ in Figure 2.4.

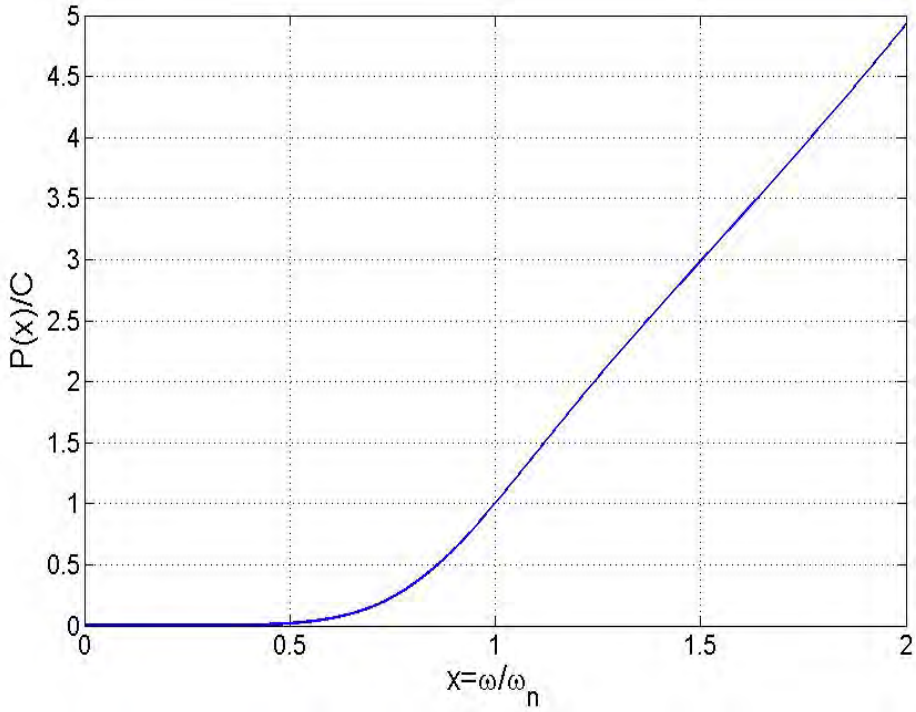

Figure 2.4: Power as a function of frequency with $\zeta = 0.5$.

Figure 2.4 shows when $\zeta = 0.5$, $\frac{P(x)}{C}$ is an increasing function of x.

For $\zeta = 0.7$,

$$P'(x) = \frac{2Cx^5\left[x^4 - 0.08x^2 + 3\right]}{\left(x^4 - 0.04x^2 + 1\right)^2}. \tag{2.34}$$

Solving $P'(x) = 0$ yields four complex roots. The critical point is $x = 0$. Now we plot $\frac{P(x)}{C}$ for $\zeta = 0.7$ in Figure 2.5

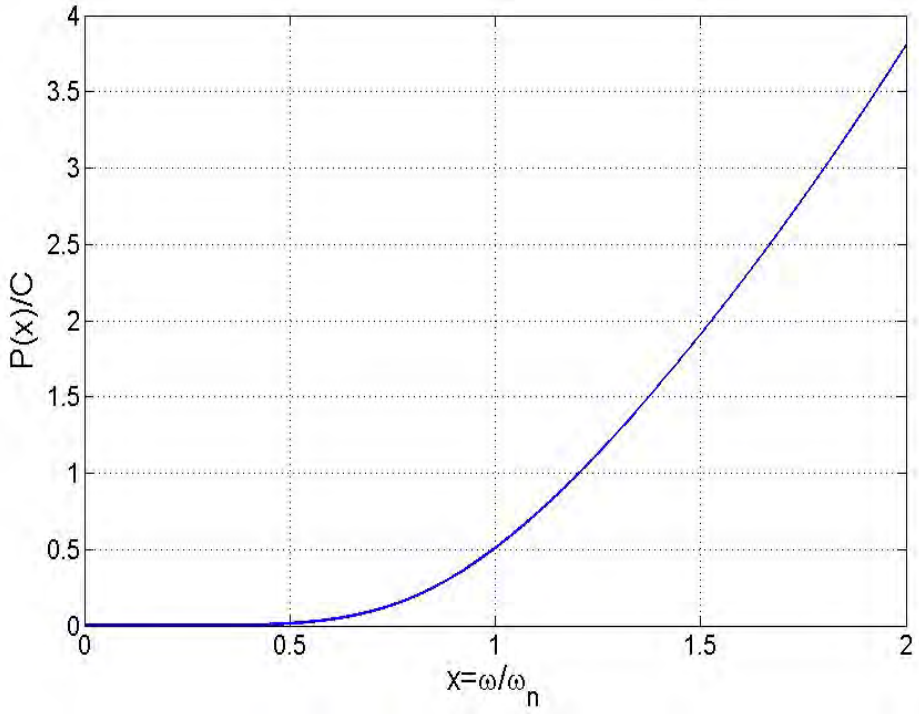

Figure 2.5: Power as a function of frequency with $\zeta = 0.7$.

Figure 2.5 shows when $\zeta = 0.7$, $\frac{P(x)}{C}$ is an increasing function of x.

2.2.2 Analysis as ζ Approaches Zero

One will notice only $\zeta = 0.1$ resulted in a critical point other than $x = 0$. Let us evaluate the critical points and corresponding optical $\frac{P(x)}{C}$ when $\zeta < 0.1$. For $\zeta = 0.05$,

$$P'(x) = \frac{2Cx^5\left[x^4 - 3.98x^2 + 3\right]}{\left(x^4 - 1.99x^2 + 1\right)^2}. \tag{2.35}$$

Solving $P'(x) = 0$ yields critical points $x = \pm 1.7233, \pm 1.0051$. For $\zeta = 0.05$, we plot $\frac{P(x)}{C}$ as a function of x in an interval containing the critical points in Figure 2.6.

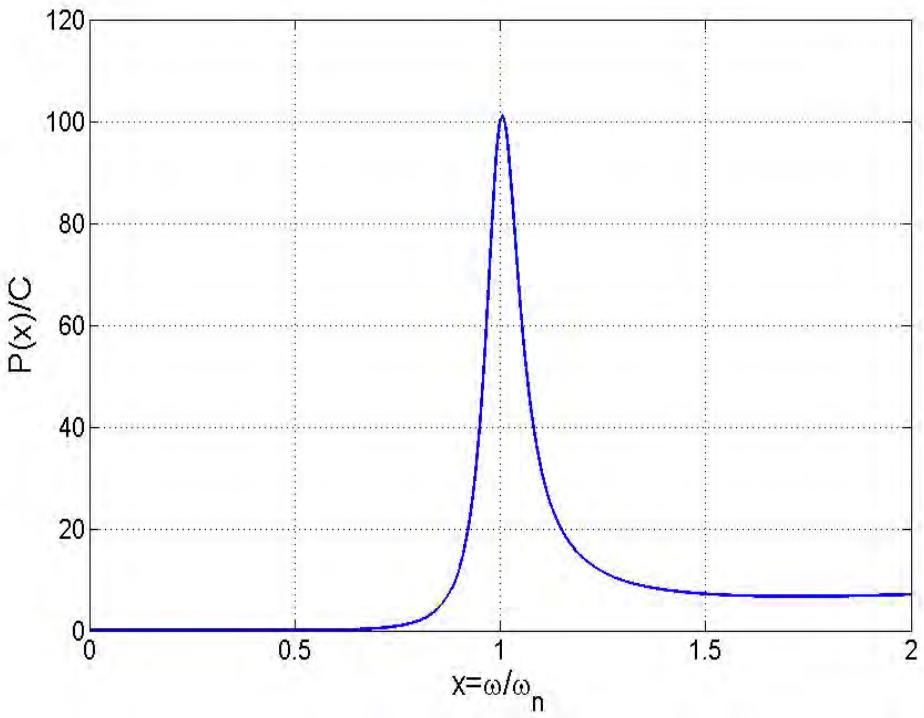

Figure 2.6: Power as a function of frequency with $\zeta = 0.05$.

From Figure 2.6, we can see that the maximum power can be generated when $x = \frac{\omega}{\omega_n} = 1.0051$ for $\zeta = 0.05$, and the maximum value of $\frac{P(x)}{C}$ is 101.01.

It appears as ζ approaches zero, the optimal value of x approaches one and the resulting maximum power generation, $\frac{P(x)}{C}$, increases. See Figures 2.7 and 2.8 for further illustration of the how the optimal x value and maximum power generation change as ζ decreases.

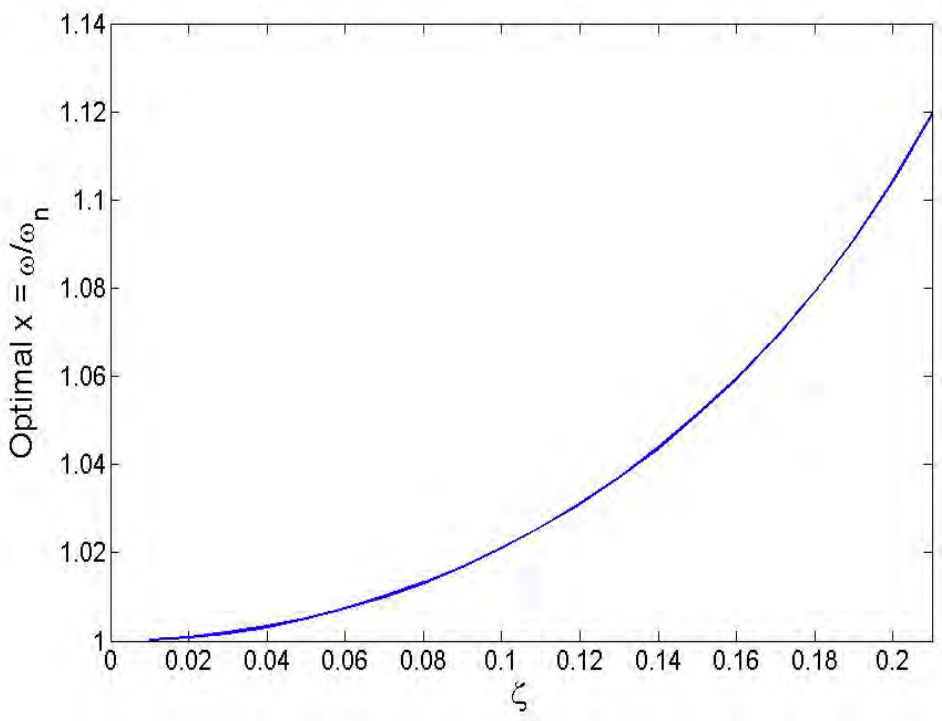

Figure 2.7: Optimal x as a function of ζ.

Figure 2.7 further depicts the optimal frequency ratio ($\frac{\omega}{\omega_n}$) approaching one as ζ approaches zero. This follows the principal of resonance, where a vibration is able to drive a system into larger oscillations when the vibration frequency matches the system's natural frequency ($\omega = \omega_n$).

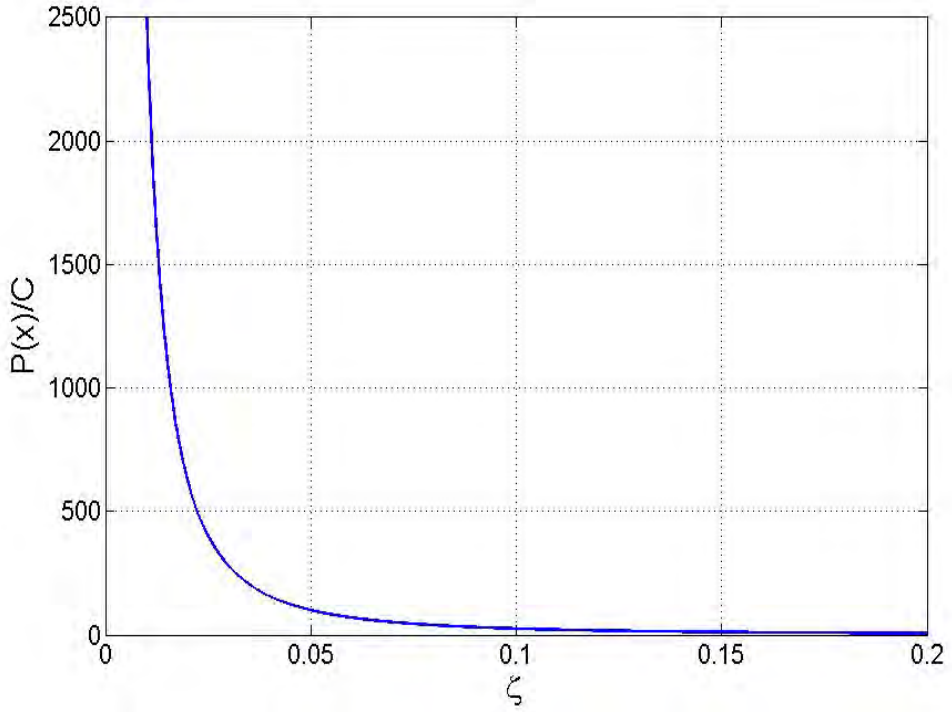

Figure 2.8: $\frac{P(x)}{C}$ as a function of ζ.

Figure 2.8 demonstrates that when we set $\omega = \omega_n$, $\frac{P(x)}{x}$ depends solely on how small we can set ζ.

2.3 Power as a Function of Modal Damping Ratio and Normalized Frequency

We will now treat net electric power generated, P, as a function of both modal damping ratio, ζ, and frequency ratio, $x = \frac{\omega}{\omega_n}$. We can graphically solve for the optimal value of $\frac{P(x)}{C}$ by plotting $\frac{P(x)}{C}$ as the dependent variable and using ζ and $x = \frac{\omega}{\omega_n}$ as the independent variables. If we use the parameters $0.1 \leq \zeta \leq 1$ and $0 < x \leq 2$, we get the plot in Figure 2.9.

From Figure 2.9 we can see the extreme value of $\frac{P(x)}{C}$ increases as ζ goes to zero and x goes to one.

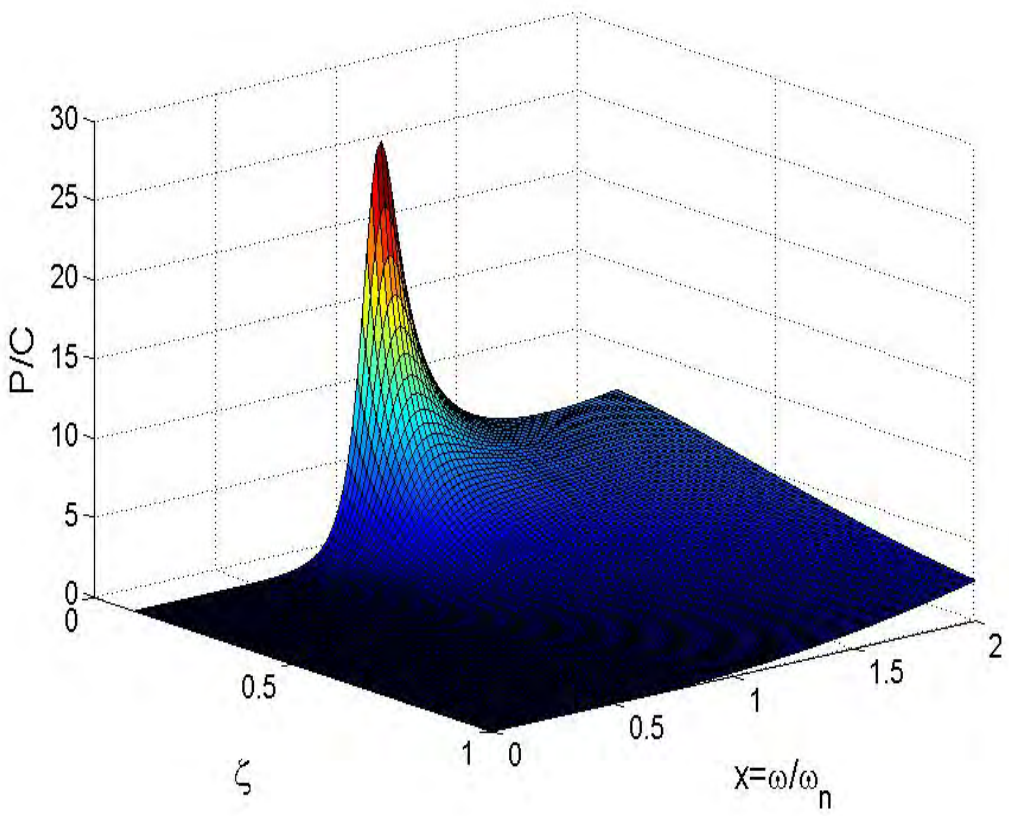

Figure 2.9: Power as a function of damping factor and frequency ($0.1 \leq \zeta \leq 1$ and $0 < x \leq 2$)

The extreme value of net electric power generated is further illustrated in Figure 2.10 with parameters $0.05 \leq \zeta \leq 1$ and $0 < x \leq 2$.

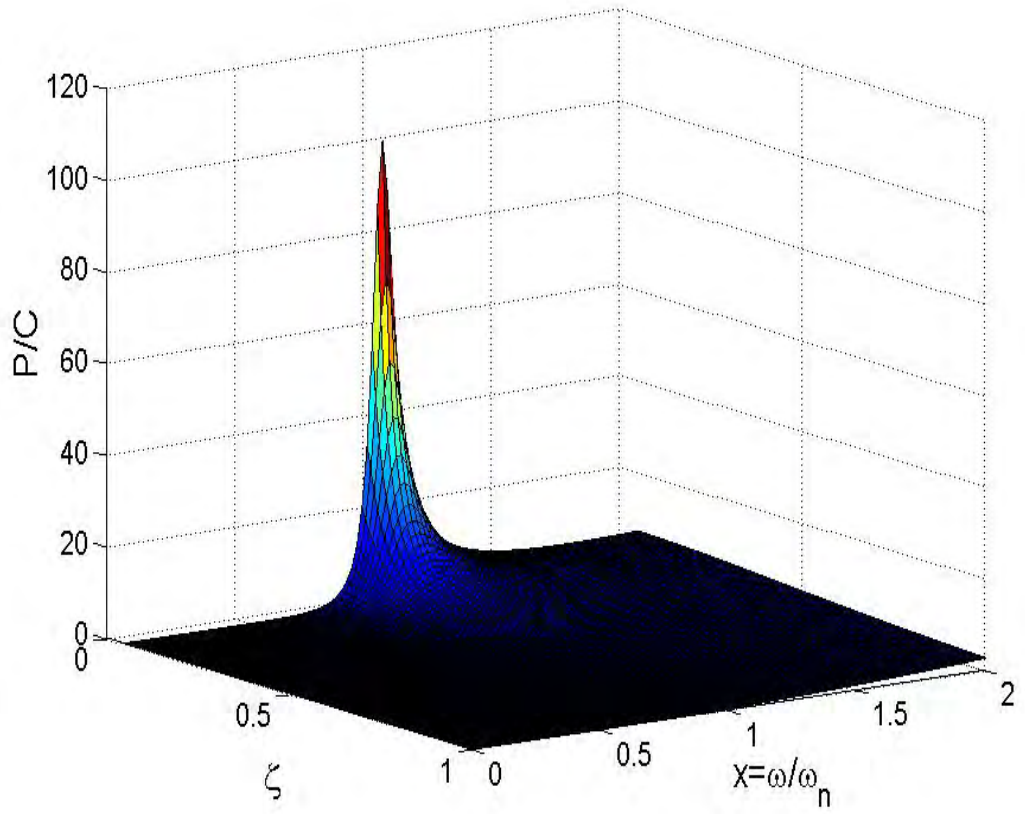

Figure 2.10: Power as a function of damping factor and frequency ($0.05 \leq \zeta \leq 1$ and $0 < x \leq 2$).

2.4 Model Comparison with Experimental Results

Roundy and Wright [15] use similar mathematical methods to design and test a piezoelectrical vibration based generator. Their design uses an 8.44 gram mass and a two-layer sheet of PZT-5A with a steel center shim excited by vibrations of $2.5m\ s^{-2}$ at $120Hz$. They assume the resonance frequency of their generator, ω_n, matches the driving frequency, ω. The damping ratio, ζ, is measured by applying an impulse to the system, and then measuring the open circuit voltage output. The resulting damped harmonic oscillation is used to calculate a damping ratio near 0.015 [15]. Figure 2.11 shows the piezoelectric generator

designed by Roundy and Wright.

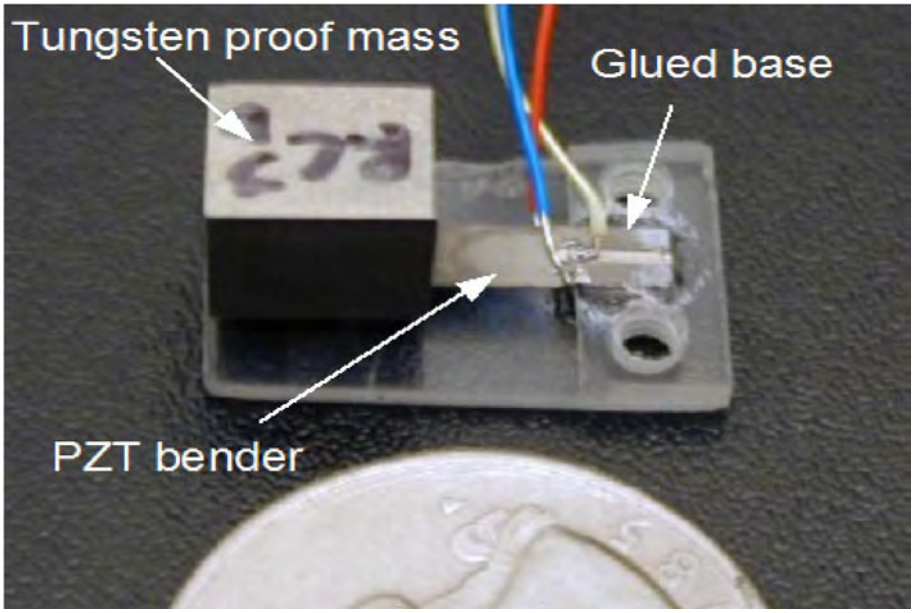

Figure 2.11: Piezoelectric generator prototype used by Roundy and Wright [15].

With these parameter values, we can compute the power generated using our ODE model. All red text below are values taken from the Roundy and Wright generator model.

$$\omega = \omega n = (2\pi)120Hz = \frac{240\pi}{second} \tag{2.36}$$

$$x = \frac{\omega}{\omega_n} = 1 \tag{2.37}$$

$$\zeta = \frac{d}{dc} = \frac{d}{2m\omega n} = 0.015 \tag{2.38}$$

$$m \approx 8.44grams = 8.44 \times 10^{-3} kg \tag{2.39}$$

$$acceleration = \frac{2.5m}{second^2} \tag{2.40}$$

$$Amplitude = Y_0 = \frac{acceleration}{\omega^2} = \frac{\frac{2.5m}{second^2}}{\left(\frac{240\pi}{second}\right)^2} = 3.518 \times 10^{-6} m \tag{2.41}$$

$$C = m\zeta Y_0^2 \omega_n^3 = (8.44 \times 10^{-3} kg)(0.015)(3.518 \times 10^{-6} m)^2 \left(\frac{240\pi}{second} \right)^3 \tag{2.42}$$

$$C = \left(\frac{1.0494 \times 10^{-6} kg \cdot m^2}{second^3} \right) \tag{2.43}$$

Substituting values given from Roundy and Wright and values calculated above into Equation (2.29), we get:

$$P(1) = \left(\frac{1.0494 \times 10^{-6} kg \cdot m^2}{second^3} \right) \frac{1}{(2(.015))^2} = \frac{1.2 \times 10^{-3} kg \cdot m^2}{second^3}. \tag{2.44}$$

The corresponding result from Roundy and Wright is

$$P(1) \approx \frac{3.75 \times 10^{-4} kg \cdot m^2}{second^3}. \tag{2.45}$$

Roundy and Wright's experiment results in power 68.75% less than our mathematical results. The disparity between our ODE model calculation and Roundy and Wright's experimental results can be explained through the fact our model is purely mechanically based and does not take into account loss of energy through the transfer of mechanical energy to electrical energy. Despite the power disparity, Roundy and Wright's results support our ODE model.

2.5 One-Dimensional Power Generation Model Conclusion

Our 1-D model shows potential to serve as a foundation to optimize power generated by a piezoelectric generator. In order to optimize power generated, $\frac{P(x)}{C}$, we should minimize the damping factor, ζ, and choose the optimizing frequency ratio, $x = \frac{\omega}{\omega_n}$. Keep in mind that as ζ approaches zero the optimal frequency ratio approaches one and the maximum power generated drastically increases.

THIS PAGE INTENTIONALLY LEFT BLANK

CHAPTER 3:
Single-Mode Model:
Derivation of the Six Variable Model

There are many studies on the transduction of electrical energy from a single piezoelectric transducer (see [18] and references therein) and the general conclusion is that piezoelectric energy harvesting approaches have considerable promise for applications involving small amounts of power [19]. To boost the power output of such system, one proposal by Scruggs [20] is to use multiple transducer patches and channel energy generated by some of the patches into other patches in order to excite additional vibration modes. An example of this type of energy harvesting system is depicted in Figure 3.1. The parameters describing the size of a piezoelectric patch take the typical values $l_1 \approx l_2 \approx l_3 = 100mm$, $w = 25mm$, $t_p = 0.25mm$ and the thickness of the beam is $t_b = 0.25mm$ [21].

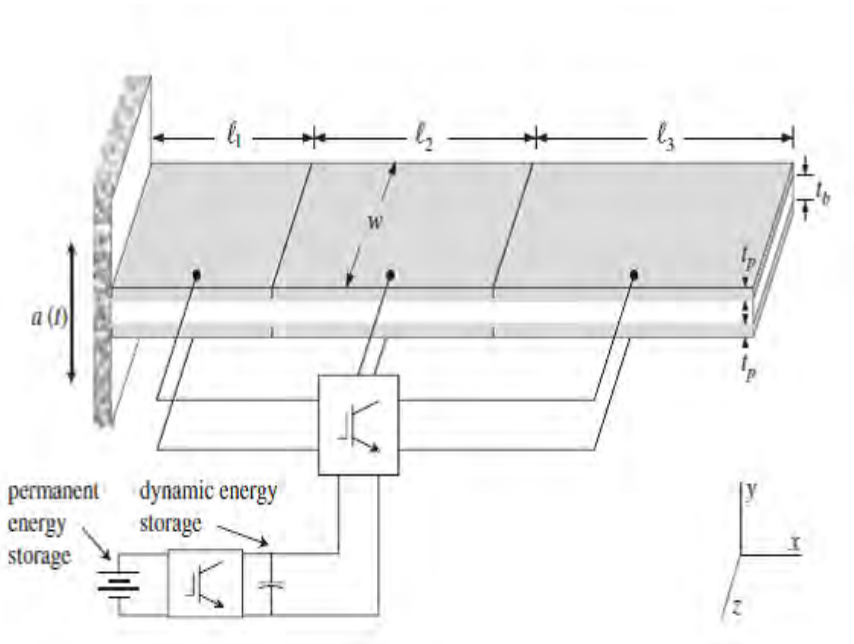

Figure 3.1: Energy harvesting bimorph cantilever with distributed piezoelectric transducers (gray) bonded to a substrate (white). Adapted from Dutoit, Wardle and Kim [16].

The general equations for linear piezoelectricity are shown in Figure 3.2.

Gauss' law : $\dfrac{\partial D_j}{\partial x_j} = \rho,$

$\boldsymbol{D}(x) = \begin{bmatrix} D_1 \\ D_2 \\ D_3 \end{bmatrix}$: a vector of electrical displacements (charge/area)

ρ: charge density

Mechanical energy balance: $\rho \dfrac{\partial^2 u_i}{\partial t^2} = \dfrac{\partial T_{ij}}{\partial x_j}$

u_i : displacement, T_{ij} : stress

Constitutive relation [2]:

$$\begin{bmatrix} D_1 \\ D_2 \\ D_3 \\ T_1 \\ T_2 \\ T_3 \\ T_4 \\ T_5 \\ T_6 \end{bmatrix} = \begin{bmatrix} \varepsilon_{11} & & & & & & e_{15} & 0 \\ & \varepsilon_{11} & & & & e_{15} & & \\ & & \varepsilon_{33} & e_{31} & e_{31} & e_{33} & & \\ & & -e_{31} & c_{11} & c_{12} & c_{13} & & \\ & & -e_{31} & c_{12} & c_{11} & c_{13} & & \\ & & -e_{33} & c_{13} & c_{13} & c_{33} & & \\ & -e_{15} & & & & & c_{55} & \\ -e_{15} & & & & & & & c_{66} \\ 0 & & & & & & & \end{bmatrix} \begin{bmatrix} E_1 \\ E_2 \\ E_3 \\ S_1 \\ S_2 \\ S_3 \\ S_4 \\ S_5 \\ S_6 \end{bmatrix}$$

$$\boldsymbol{S}(x) = \begin{bmatrix} S_{11} \\ S_{22} \\ S_{33} \\ 2S_{23} \\ 2S_{13} \\ 2S_{12} \end{bmatrix} = \begin{bmatrix} S_1 \\ S_2 \\ S_3 \\ S_4 \\ S_5 \\ S_6 \end{bmatrix} \text{ material strains, } \boldsymbol{T}(x) = \begin{bmatrix} T_{11} \\ T_{22} \\ T_{33} \\ T_{23} \\ T_{13} \\ T_{12} \end{bmatrix} = \begin{bmatrix} T_1 \\ T_2 \\ T_3 \\ T_4 \\ T_5 \\ T_6 \end{bmatrix} \text{ material stress (force/area),}$$

$\boldsymbol{E}(x) = \begin{bmatrix} E_1 \\ E_2 \\ E_3 \end{bmatrix}$ electrical field in the material (volts/meter)

e_{ij} : coupling coefficients ε_{ij} : dielectric constants c_{ij} : modulus of elasticity

Figure 3.2: General equations for linear piezoelectricity [20].

The constitutive relation in Figure 3.2 is for material that is electrically and mechanically isotropic in the 1 and 2 directions, while the 3-direction is the poling direction. The first three rows of the constitutive relation relate the electrical displacement to the electrical field and to the strain in the material, and the remaining six rows relate the mechanical stress to the electric field and to the strain. Here the stress, $T(x)$, and strain, $S(x)$, are represented in Voigt notation or Voigt form. Referring to the Figure 3.1 above, 1 corresponds to x and 3 corresponds to y.

Equations for a patch on a beam are largely based on Euler-Bernoulli (or Timoshenko) beam models. Piezoelectric layers or patches are bonded to the both sides of the beam. The beam is assumed to be in pure bending; all other deformations are considered negligible. Here we consider a "bimorph" configuration. That is, in the undisturbed state the beam lies along the x-axis in $a < x < b, -\frac{t_b}{2} < y < \frac{t_b}{2}, -\frac{w}{2} < z < \frac{w}{2}$, with equal patches on its upper and lower surfaces $y = \pm\frac{t_b}{2}$, each of thickness t_p and covering the entire upper and lower surfaces. It is further assumed that the patches are bonded perfectly to the substructure and the electrodes cover their entire upper and lower surface areas. The beam is clamped, at $x = a$, on a base that is subject to motion in the y-direction; it is free at $x = b$. The polar direction on the top patch is in the y-direction and on the bottom patch it is reversed so that the voltages on the two patches add. Due to this asymmetry, we can compute the piezoelectric effect on the upper patch alone and double the result.

Adopting the standard assumptions of Euler-Bernoulli beam theory, a balance of forces and moments can be combined to yield

$$-M_{xx} = m\left(\omega_{tt} + h_{tt}\right). \tag{3.1}$$

where $M(x,t)$ is the internal moment generated by mechanical and electrical strain, m is the mass per unit length of the composite beam, ω is the relative vertical deflection along the beam from the base, and h is the absolute motion of the base/host structure (thus $w+h$ is the absolute displacement of the beam). The Euler-Bernoulli bending deformation model relates the stress to the curvature of the beam:

$$S_1 = -y\omega_{xx} \tag{3.2}$$

The constitutive relations yield $T_1 = c_{11}S_1 \mp e_{31}E_3, \quad D_3 = \pm e_{31}S_1 + e_{33}E_3$ (the sign of the coupling terms may vary from patch to patch depending on whether they are poled in the positive y or negative y direction). Additionally, it is assumed that the electrical field is constant throughout the thickness of the patches; therefore, $E_3 = \pm\frac{v_p}{t_p}$ with the sign depending on the poling direction, where v_p is the terminal voltage on the top of the top patch with thickness t_p.

The relation between moment and stress is:

$$M = -w\int_{-\frac{t_b}{2}}^{\frac{t_b}{2}} T_1 y dy - w\left[\int_{\frac{t_b}{2}}^{\frac{t_b}{2}+t_p} T_1 y dy + \int_{-\frac{t_b}{2}-t_p}^{-\frac{t_b}{2}} T_1 y dy\right]\left[H(x-a) - H(x-b)\right], \tag{3.3}$$

$$M = c_{11}w\frac{{t_b}^3}{12}\omega_{xx} - e_{31}w\frac{t_b+t_p}{2}\left[H(x-a) - H(x-b)\right]v_p \cdot 2, \tag{3.4}$$

where w is the width of both the beam and the piezo patches and H denotes the Heaviside step function.

When the electric field is normal to the beam axis and uniform in the patch over $a < x < b$ and zero outside this interval, the piezoelectric effect contribution to the displacement equation enters as derivatives of delta functions at the ends of each patch [22]:

$$m\omega_{tt} + \left(c_{11}w\frac{{t_b}^3}{12}\right)\omega_{xxxx} + e_{31}w(t_b+t_p)\left[\delta'(x-b) - \delta'(x-a)\right]v_p = -mh_{tt}. \tag{3.5}$$

The boundary conditions for equation (3.5) are $\omega(a,t) = \omega_x(a,t) = 0$. This reflects the fact that the beam is clamped at $x = a$, but at the free end, $x = b$, we have $M = M_x = 0$. The size of the charge can be found by integrating the Gauss' law over the surface area of the electrodes [22]:

$$q(t) = \iint_{upper} D_3 dA - \iint_{lower} D_3 dA = e_{31}w(t_p+t_s)\left[\omega_x\right]\Big|_a^b - \frac{2\varepsilon_{33}}{t_p}w(b-a)v_p\,. \tag{3.6}$$

Equations (3.5) and (3.6) provide a complete system of equations for the vibration energy harvester. The most common method of solving the system (3.5-3.6) is to assume that the

beam deflection can be represented by an eigenfunction expansion

$$\omega(x,t) = \sum_{i=1}^{\infty} \phi_i(x)\, u_i(t), \tag{3.7}$$

where $\phi_i(x)$ is the i-th mode shape function and $u_i(t)$ is the i-th modal displacement. The mode shape functions must satisfy the boundary conditions and follow the following orthogonality relationships:

$$\int_a^b \phi_i(x)\, \phi_j(x)\, dx = \delta_{ij}. \tag{3.8}$$

Substituting (3.7) into (3.5), multiplying both sides by $\phi_k(x)$, and integrating x from a to b yields for each k, we arrive at

$$u_k''(t) + \left[{w_{SC,k}}^2\right] u_k + A_k v_p = -m\,[\gamma_k]\, h''(t), \tag{3.9}$$

where Equation (3.10) is the modal short-circuit frequency, Equation (3.11) is the modal electromechanical coupling coefficient, and Equation (3.12) is the modal influence coefficient of the base excitation.

$$w_{SC,k} = {\lambda_k}^2 \sqrt{\frac{c_{11} w {t_b}^3}{12m(b-a)^4}} \tag{3.10}$$

where λ_k is the eigenvalue corresponding to $\phi_k(x)$; for cantilevered configurations, these numbers are the solutions to $\cos(\lambda)\cosh(\lambda) = 1$

$$A_k = e_{31} w\,(t_b + t_p)\left[{\phi_k}'(x-b) - {\phi_k}'(x-a)\right], \tag{3.11}$$

$$\gamma_k = \int_a^b \phi_k(x)\, dx. \tag{3.12}$$

At this point, it is common to add in a modal damping term $2w_{SC,k}\zeta_k {u_k}'(t)$ to the left side of Equation (3.9) to account for all proportional damping effects. Four possible damping mechanisms, one external and three internal, and various combinations of these mechanisms have been considered by Banks and Inman [23]. They are viscous air damping, strain

rate damping or Kelvin-Voigt damping, spatial hysteresis, and time hysteresis, respectively. Their study shows that air damping plays a more significant role in lower modes whereas internal damping plays a more important role for higher modes.

Equations (3.9) and (3.6) provide a complete system of equations for the vibration energy harvester. If the beam is excited with a driving frequency that is close to one of its natural frequencies, then the corresponding mode of that frequency will dominate the motion of the beam. In this situation, it is reasonable to make the approximation $\omega(x,t) = \sum_{i=1}^{\infty} \phi_i(x)\, u_i(t) \approx \phi_1(x)\, u_1(t)$. After we drop the "1" subscript, this simple approximation reduces Equation 3.9 to

$$u''(t) + 2w_{SC}\zeta u'(t) + \left[{w_{SC}}^2\right] u + Av_p = -m[\gamma] h''(t). \tag{3.13}$$

Here m is the mass/unit length, γ is the modal influence coefficient of the base excitation, ζ is the modal damping ratio, w_{SC} is the modal short-circuit natural frequency, and A is the electromechanical coupling coefficient (effective piezoelectric constant). Equation (3.6) is simplified to

$$q(t) = e_{31} w (t_p + t_s) [\phi_x u] \Big|_a^b - \frac{2\varepsilon_{33}}{t_p} w (b-a)\, v_p\,. \tag{3.14}$$

Differentiating Equation (3.14) yields

$$-Au' + \frac{2\varepsilon_{33}}{t_p} w (b-a)\, {v_p}' = -i, \tag{3.15}$$

where i represents the current. We can focus on the single-mode model (Equations (3.13) and (3.15)) for now, which assumes that the beam is vibrating near its fundamental natural frequency and, consequently, the motion of the beam is described by one modal coordinate (typically, the fundamental mode). We need to solve the system and find the maximum power points of energy harvesting over a range of base excitation frequencies, patch thickness and length, load resistances, etc. The results will allow a designer to choose the optimal resonant frequency and patch dimensions to maximize the power harvested.

In the single-mode model, i.e., Equations (3.13) and (3.15), the two unknowns are the modal displacement $u(t)$ and the terminal voltage v_p, and the two inputs are the base motion

$h(t)$ and the current i. The beam tip deflection, which is a predominant measure, can be computed by the simple relation $\omega(L,t) = \phi(L)u(t)$, where $\phi(x)$ is the fundamental mode shape function. The coefficients of Equations (3.13) and (3.15) can be calculated using knowledge of the materials and the layout of the beam, or they may be estimated experimentally.

The most commonly analyzed scenario for vibration energy harvesting is steady state base excitation. At steady state, we suppose that the beam and base motions are of the following forms, respectively

$$u(t) = U\sin(\omega_{base}t), \tag{3.16}$$

$$h(t) = H\sin(\omega_{base}t - \phi_{base}), \tag{3.17}$$

where U is the amplitude of the modal displacement, H is the amplitude of the base motion, ω_{base} is the base motion driving frequency, and ϕ_{base} is the phase lead of the base motion relative to the beam motion. If we further consider a simple resistive load where $i = \frac{v_p}{R}$ and R is the load resistance, then Equations (3.13) and (3.15) are simplified to a linear system. Assuming the voltage signal takes the form $v_p = V_p\sin(\omega_{base}t - \theta_{voltage})$ and substituting these expressions into Equation (3.15), we have

$$-AU\omega_{base}\cos(\omega_{base}t) + C_0V_p\omega_{base}\cos\left(\omega_{base}t - \theta_{voltage}\right) = -\frac{V_p\sin\left(\omega_{base}t - \theta_{voltage}\right)}{R}, \tag{3.18}$$

where $C_0 \equiv \frac{2\varepsilon_{33}}{t_p}w(b-a)$. With the help of trigonometric identities $\cos(x-y) = \cos x\cos y + \sin x\sin y$ and $\sin(x-y) = \sin x\cos y - \cos x\sin y$ we can rewrite Equation (3.18) as

$$\begin{aligned} -AU\omega_{base}\cos(\omega_{base}t) + C_0V_p\omega_{base}&\left[\cos(\omega_{base}t)\cos\theta_{voltage} + \sin(\omega_{base}t)\sin\theta_{voltage}\right] \\ &= -\frac{V_p}{R}\left[\sin(\omega_{base}t)\cos\theta_{voltage} - \cos(\omega_{base}t)\sin\theta_{voltage}\right]. \end{aligned} \tag{3.19}$$

Matching the coefficients of $\cos(\omega_{base}t)$ and $\sin(\omega_{base}t)$ respectively, we obtain

$$-AU\omega_{base} + C_0V_p\omega_{base}\cos\theta_{voltage} = \frac{V_p}{R}\sin\theta_{voltage}. \tag{3.20}$$

Solving for $\cos\theta_{voltage}$, we obtain

$$\cos\theta_{voltage} = -C_0\omega_{base}R\sin\theta_{voltage}. \tag{3.21}$$

Substituting Equation (3.21) into Equation (3.20), we get

$$-AU\omega_{base}+C_0V_p\omega_{base}\left(-C_0\omega_{base}R\sin\theta_{voltage}\right)=\frac{V_p}{R}\sin\theta_{voltage}. \tag{3.22}$$

Solving for $\sin\theta_{voltage}$, we obtain

$$\sin\theta_{voltage}=-\frac{AU\omega_{base}R}{V_p\left(1+{C_0}^2{\omega_{base}}^2R^2\right)}. \tag{3.23}$$

Substituting Equation (3.23) into Equation (3.21) yields

$$\cos\theta_{voltage}=\frac{C_0AU{\omega_{base}}^2R^2}{V_p\left(1+{C_0}^2{\omega_{base}}^2R^2\right)}. \tag{3.24}$$

Now substituting Equations (3.23) and (3.24) into Equation (3.13)

$$\begin{aligned}&-U{\omega_{base}}^2\sin\left(\omega_{base}t\right)+2w_{SC}\zeta U\omega_{base}\cos\left(\omega_{base}t\right)\\&+\left[{w_{SC}}^2\right]U\sin\left(\omega_{base}t\right)+AV_p\sin\left(\omega_{base}t-\theta_{voltage}\right)\\&=m\left[\gamma\right]H{\omega_{base}}^2\sin\left(\omega_{base}t-\phi_{base}\right),\end{aligned} \tag{3.25}$$

which leads to

$$\begin{aligned}&-U{\omega_{base}}^2\sin\left(\omega_{base}t\right)+2w_{SC}\zeta U\omega_{base}\cos\left(\omega_{base}t\right)+\left[{w_{SC}}^2\right]U\sin\left(\omega_{base}t\right)\\&+AV_p\left[\sin\left(\omega_{base}t\right)\cos\theta_{voltage}-\cos\left(\omega_{base}t\right)\sin\theta_{voltage}\right]\\&=m\left[\gamma\right]H{\omega_{base}}^2\left[\sin\left(\omega_{base}t\right)\cos\phi_{base}-\cos\left(\omega_{base}t\right)\sin\phi_{base}\right].\end{aligned} \tag{3.26}$$

Matching the coefficients of $\cos(\omega_{base}t)$ and $\sin(\omega_{base}t)$, respectively, we get

$$-U{\omega_{base}}^2+\left[{w_{SC}}^2\right]U+AV_p\cos\theta_{voltage}=m\left[\gamma\right]H{\omega_{base}}^2\cos\phi_{base}, \tag{3.27}$$

$$2w_{SC}\zeta U\omega_{base}-AV_p\sin\theta_{voltage}=-m\left[\gamma\right]H{\omega_{base}}^2\sin\phi_{base}. \tag{3.28}$$

Substituting Equation (3.21) into Equation (3.27), we obtain

$$-U{\omega_{base}}^2+\left[{w_{SC}}^2\right]U+AV_p\frac{C_0AU{\omega_{base}}^2R^2}{V_p\left(1+{C_0}^2{\omega_{base}}^2R^2\right)}=m\left[\gamma\right]H{\omega_{base}}^2\cos\phi_{base}. \tag{3.29}$$

Solving for $\cos\phi_{base}$, we find

$$\cos\phi_{base} = \frac{-{\omega_{base}}^2 + \left[{w_{SC}}^2\right] + \frac{C_0 A^2 {\omega_{base}}^2 R^2}{\left(1+{C_0}^2{\omega_{base}}^2 R^2\right)}}{m\left[\gamma\right] H {\omega_{base}}^2} U. \tag{3.30}$$

Substituting Equation (3.23) into Equation (3.28), we obtain

$$2 w_{SC}\zeta U\omega_{base} + AV_p \frac{AU\omega_{base}R}{V_p\left(1+{C_0}^2{\omega_{base}}^2R^2\right)} = -m\left[\gamma\right]H{\omega_{base}}^2\sin\phi_{base}. \tag{3.31}$$

Solving for $\sin\phi_{base}$, we find

$$\sin\phi_{base} = -\frac{2 w_{SC}\zeta\omega_{base} + \frac{A^2\omega_{base}R}{\left(1+{C_0}^2{\omega_{base}}^2R^2\right)}}{m\left[\gamma\right]H{\omega_{base}}^2} U. \tag{3.32}$$

Using Equations (3.30) and (3.32) and the trigonometric identity $\cos^2(\phi_{base}) + \sin^2(\phi_{base}) = 1$, we find

$$\left[\frac{-{\omega_{base}}^2 + \left[{w_{SC}}^2\right] + \frac{C_0 A^2 {\omega_{base}}^2 R^2}{\left(1+{C_0}^2{\omega_{base}}^2 R^2\right)}}{m\left[\gamma\right] H {\omega_{base}}^2}\right]^2 U^2 + \left[-\frac{2 w_{SC}\zeta\omega_{base} + \frac{A^2\omega_{base}R}{\left(1+{C_0}^2{\omega_{base}}^2R^2\right)}}{m\left[\gamma\right]H{\omega_{base}}^2}\right]^2 U^2 = 1. \tag{3.33}$$

Solving for U leads to

$$U = \frac{m[\gamma]H{\omega_{base}}^2\left(1+{C_0}^2{\omega_{base}}^2R^2\right)}{\sqrt{\left(\left(-{\omega_{base}}^2+\left[{w_{SC}}^2\right]\right)\left(1+{C_0}^2{\omega_{base}}^2R^2\right)+C_0A^2{\omega_{base}}^2R^2\right)^2+\left(2w_{SC}\zeta\omega_{base}\left(1+{C_0}^2{\omega_{base}}^2R^2\right)+A^2\omega_{base}R\right)^2}}. \tag{3.34}$$

Using Equations (3.23) and (3.24) and the trigonometric identity $\cos^2(\theta_{voltage}) + \sin^2(\theta_{voltage}) = 1$, we obtain

$$\left[-\frac{AU\omega_{base}R}{V_p\left(1+{C_0}^2{\omega_{base}}^2R^2\right)}\right]^2 + \left[\frac{C_0AU{\omega_{base}}^2R^2}{V_p\left(1+{C_0}^2{\omega_{base}}^2R^2\right)}\right]^2 = 1. \tag{3.35}$$

Solving for V_p, we find

$$V_p = AU\omega_{base}R. \tag{3.36}$$

Substituting Equation (3.34) into Equation (3.36), we obtain

$$V_p = \frac{ARm[\gamma]H{\omega_{base}}^3\left(1+{C_0}^2{\omega_{base}}^2R^2\right)}{\sqrt{\left(\left(-{\omega_{base}}^2+\left[{w_{SC}}^2\right]\right)\left(1+{C_0}^2{\omega_{base}}^2R^2\right)+C_0A^2{\omega_{base}}^2R^2\right)^2+\left(2w_{SC}\zeta\omega_{base}\left(1+{C_0}^2{\omega_{base}}^2R^2\right)+A^2\omega_{base}R\right)^2}}. \tag{3.37}$$

The average power dissipated by the load resistor is given by

$$P = \frac{V_p^2}{2R}. \tag{3.38}$$

Substituting Equation (3.37) into Equation (3.38), we obtain an expression for power:

$$P = \frac{A^2Rm^2[\gamma]^2H^2{\omega_{base}}^6\left(1+{C_0}^2{\omega_{base}}^2R^2\right)^2}{2\left[\left(\left(-{\omega_{base}}^2+\left[{w_{SC}}^2\right]\right)\left(1+{C_0}^2{\omega_{base}}^2R^2\right)+C_0A^2{\omega_{base}}^2R^2\right)^2+\left(2w_{SC}\zeta\omega_{base}\left(1+{C_0}^2{\omega_{base}}^2R^2\right)+A^2\omega_{base}R\right)^2\right]}. \tag{3.39}$$

Equation (3.39) provides an explicit and complicated form for power generation, which involves nine parameters. We will study the effects of these parameters in the following chapters.

CHAPTER 4:
Optimization Methodology

4.1 Optimization Methodology Overview

We optimize piezoelectric power generation by analyzing two power generation models using two sampling approaches and one iterative approach. The goal of our methodology is to discover the optimal values of each variable in order to maximize power generation. In the following chapter we compare the results of each optimization method and analyze the robustness of our results.

4.2 Power Generation Models

We optimize piezoelectric power generation by optimizing the mathematical models described in Chapters 2 and 3. We attempt to find the optimal combination of variable values in order to maximize power.

The first model is an adaptation of Equation (2.28). It consists of three variables, ω, ω_n, and ζ. We will not consider m or Y_0^2 as they occur only in the numerator of Equation (2.28) and obviously maximize power by taking on the largest value possible:

$$\frac{P}{mY_0{}^2} = \frac{\zeta(\frac{\omega}{\omega_n})^3\omega^3}{(1-\frac{\omega^2}{\omega_n^2})^2+(2\zeta\frac{\omega}{\omega_n})^2} \tag{4.1}$$

The second model is an adaptation of Equation (3.39). It consists of six variables. We will not consider m, γ, or H as they occur only in the numerator of Equation (3.39) and obviously maximize power by taking on the largest value possible:

$$\frac{P}{(m\gamma H)^2} = \frac{A^2R{\omega_{base}}^6(1+{C_0}^2{\omega_{base}}^2R^2)^2}{2[((-{\omega_{base}}^2+{w_{SC}}^2)(1+{C_0}^2{\omega_{base}}^2R^2)+C_0A^2{\omega_{base}}^2R^2)^2+(2w_{SC}\zeta\omega_{base}(1+{C_0}^2{\omega_{base}}^2R^2)+A^2\omega_{base}R)^2]} \tag{4.2}$$

Equations (4.1) and (4.2) lie in the core of our analysis.

4.3 Variable Ranges

In order to optimize maximum power generated we must constrain our variables. The goal of the optimization is to find the optimum combination of variables in order to maximize power and lead to the development of more efficient piezoelectric generators. Keeping in mind the practical application of our optimization, we select the ranges of each variable in such a way that engineers will be able to select materials and conditions within the limits of each variable to create a physical model based on our results. Figures 4.1 and 4.2 display the ranges for variables in Equations (4.1) and (4.2), respectively.

Table 4.1: Variable ranges for the three-variable power generation model of Equation (4.1).

Variable	Variable Symbol	Range
Frequency of Excitation	ω	$[120\pi s^{-1}, 360\pi s^{-1}]$
Natural Frequency	ω_n	$[120\pi s^{-1}, 360\pi s^{-1}]$
Modal Damping Ratio	ζ	$[0.005, 0.02]$

In Roundy and Wright's experiment [15], they use the values $\omega = \omega_n = 240\pi s^{-1}$ and $\zeta = 0.015$. We choose the range of ω, ω_n and ζ by varying Roundy and Wright's experimental values.

Table 4.2: Variable ranges for the six-variable power generation model of Equation (4.2).

Variable	Variable Symbol	Range
Electromechanical Coupling Coefficient	A	$[0.01, 0.99]$
Load Resistance	R	$[0.02\Omega, 100\Omega]$
Base Motion Driving Frequency	ω_{base}	$[120\pi s^{-1}, 360\pi s^{-1}]$
Net Clamped Cap. of Piezoelectric Material	C_0	$[1 \times 10^{-8}F, 1 \times 10^{-6}F]$
Modal Short Circuit Net Frequency	w_{SC}	$[120\pi s^{-1}, 360\pi s^{-1}]$
Modal Damping Ratio	ζ	$[0.005, 0.02]$

We choose the range of ω_{base} and ζ by varying the experimental values found in Roundy and Wright's paper [15]. Likewise, we choose the range of C_0 by varying the value cited in Fleming and Behren's paper [24]. We choose to use the same range for w_{SC} as the other frequency, ω_{base}. For the coefficient, A, we use $[0.01, 0.99]$. Finally, the range of

R varies from the resistance of a copper wire to about half the resistance of an operating incandescent light bulb.

4.4 m^k Factorial Sampling

One method to find an optimal solution for power generation using our models is to evaluate the combination of all independent variables, which we will interchangeably refer to as *factors* in this chapter, at different levels. Levels are the variety of values a factor may assume in a simulation. This methodology can be described as m^k factorial design, where m is the number of levels per factor and k is the number of factors. In an m^k factorial design the number of design points is equal to m^k. Design points are the combination of factor levels to be evaluated in the simulation. The larger the value of m for an m^k factorial design, the better its space-filling properties [25]. However, an increase of levels may drastically increase the number of design points required to evaluate in a simulation.

4.5 Nearly Orthogonal and Balanced Latin Hypercube Sampling

An alternate and more efficient sampling methodology is to use space-filling designs to thoughtfully choose the specific levels of each factor to evaluate. Latin hypercube designs provide a flexible way of constructing efficient designs for qualitative factors. They have some of the space-filling properties of m^k factorial design, but require orders of magnitude less sampling [25].

K.Q. Ye [1998] describes Latin hypercubes as follows:

> An $n \times d$ Latin hypercube consists of d permutations of $S_n = \{1, 2, ...n\}$. A Latin hypercube design takes row vectors as the experimental points in a d-dimensional space. One-dimensional projections of a Latin hypercube design are evenly spaced and have the lowest possible discrepancy. [26]

The significant benefits of the Latin hypercube sampling used in this paper is the samplings' orthogonality and space-filling property.

4.6 Sampling Metric: Orthogonality

The correlation between two vectors $\vec{u} = [u_1, u_2, ...u_n]$ and $\vec{v} = [v_1, v_2, ...v_n]$ is defined the value of the quotient

$$\frac{\sum(v_i - \bar{v})(u_i - \bar{u})}{\sqrt{\sum(u_i - \bar{u})^2 \sum(v_i - \bar{v})^2}}, \tag{4.3}$$

where $\bar{u} = \frac{\sum u_i}{n}$ and $\bar{v} = \frac{\sum v_i}{n}$. If $\vec{u}$ and $\vec{v}$ are uncorrelated they are said to be orthogonal and their correlation value is zero. Alternatively, two completely correlated vectors have a correlation value of one. Orthogonal Latin hypercubes create column vectors with zero correlation [26].

Orthogonality in variable sampling is particularly valuable in regression analysis and simulations where one desires independent variables in a regression model to be orthogonal to each other in order to minimize variable correlation [27], [28]. Additionally, the orthogonal Latin hypercube design ensures independence of estimates of linear effects of each variable [26].

No matter how many levels or factors, m^k factorial samplings result in completely orthogonal design points. In other words, the design columns in factorial design are uncorrelated.

We use a select set of columns from a nearly orthogonal and balanced (NOB) design, developed by H. Vieira Jr. [29], in order to reduce the number of design points necessary to efficiently find the optimal solution to our power generation problem. After we input our model variables, with associated variable ranges, Vieira's NOB design spreadsheet outputs 512 nearly orthogonal and balanced design points [30]. According to Vieira,

> Nearly orthogonal means that the maximum absolute pairwise correlation between and two design columns is minimal. Nearly balanced means that for any single factor column, the number of occurrences of each distinct factor level is nearly equal.

Vieira and Sanchez call a design nearly orthogonal if the absolute pairwise correlation between any two factors is less than 0.05. Likewise, they call a design nearly balanced if the number of objects in each level of each factor differs from the ideal by no more than 20% [25].

The balance is a concern when discrete-valued factors with limited numbers of levels are present because rounding the levels appropriate for continuous-valued factors may induce correlations that are larger than desired. Because the designs we use in this paper involve only continuous-valued factors, hence the subset of columns is a Latin hypercube, we will refer to these as nearly orthogonal and balanced Latin hypercube (NOBLH) designs.

Below are the correlation between factors for the nearly orthogonal and balanced Latin hypercube sampling, consisting of the 512 design points generated by Vieira's NOB Design Spreadsheet. Refer to Appendix, Section A.1 and Section A.2 to see the MATLAB code we used to generate orthogonality values cited in Tables 4.3 and 4.4.

Table 4.3: Orthogonality of three-variable NOB Latin hypercube design.

	ω	ω_n	ζ
ω		-0.0011	-0.005
ω_n	- 0.0011		-0.0038
ζ	-0.005	-0.0038	

Table 4.4: Orthogonality of six-variable NOB Latin hypercube design.

	A	R	ω_{base}	C_0	w_{SC}	ζ
A		-0.00106	-0.0036	-0.00293	0.001528	0.001367
R	-0.00106		-0.0038	-0.00267	-0.00195	-0.00169
ω_{base}	-0.00359	-0.00378		-0.0017	0.002429	0.001984
C_0	-0.00293	-0.00267	-0.0017		-0.00253	-0.00179
w_{SC}	0.001528	-0.00195	0.00243	-0.00253		0.006878
ζ	0.001367	-0.00169	0.00198	-0.00179	0.006878	

Recall that perfect orthogonality is defined as having a correlation value of zero. Notice the minimum absolute pairwise correlation between each design column. Using our variable inputs, Vieira's NOBLH design produces close to orthogonal design columns for both our three- and six-variable models.

4.7 Sampling Metric: Space-Filling Property

It is desirable to select sample design points with good space-filling properties, in other words, design points distributed throughout the entire experimental region. For this paper we rate the space-filling of the samplings using the Euclidean Maximin (*Mm*) distance.

> For a given design, define a distance list $\mathbf{d} = (d_1, d_2, ..., d_{[n(n-1)]/2})$, where the elements of **d** are the Euclidean inter-site distance of the n design points, ordered from smallest to largest. The Euclidean *Mm* distance is defined as d_1, where a larger value is better. A large value of d_1 means that no two points are close to (within d_1 of) each other. [27]

We use the Equation (4.4) to compute the Euclidean *Mm* distance:

$$d(\mathbf{s},\mathbf{t}) = \sqrt{\sum_{j=1}^{k} |s_j - t_j|^2} \tag{4.4}$$

where the design space is an $n \times k$ matrix and **s** and **t** are any two design points [31].

When comparing the Euclidean *Mm* distance of two samples with equal number of design points, it is possible to depend solely on Equation (4.4). However, m^k factorial and NOBLH designs result in differing numbers of design points. NOBLH designs result in 512 design points, while the number of m^k factorial design points is a function of levels (m) and factors (k). For this Euclidean *Mm* distance calculation we use a three-variable factorial design with 10 levels and a six-variable factorial design with five levels, resulting in 1000 and 15,625 design points, respectively.

In order to compare Euclidean *Mm* distance of NOBLH and m^k factorial designs, we first normalize the design columns of each design with values from the m^k factorial design. After column normalization, it is possible to use Equation (4.4) to compute the Euclidean *Mm* distance and compare the results. Refer to Appendix, Section A.3 for our Euclidean Maximin Distance Code.

The three-variable and six-variable NOBLH designs result in Euclidean *Mm* distances of 0.018 and 0.1947, respectively. The three- and six-variable m^k factorial designs result

in Euclidean Mm distances of 0.1111 and 0.25, respectively. In both the three- and six-variable models, the m^k factorial designs provide space-filling properties optimal to the NOBLH designs.

Of course, another way of judging the space-filling property of a design is by observing the location of the design points in reference to the factor ranges. Unfortunately, this visual technique is only possible in three dimensions or below. See Figure 4.1 for a visual depiction of the 1000 design points evaluated using 10 levels (m) for the three-factor (k) model.

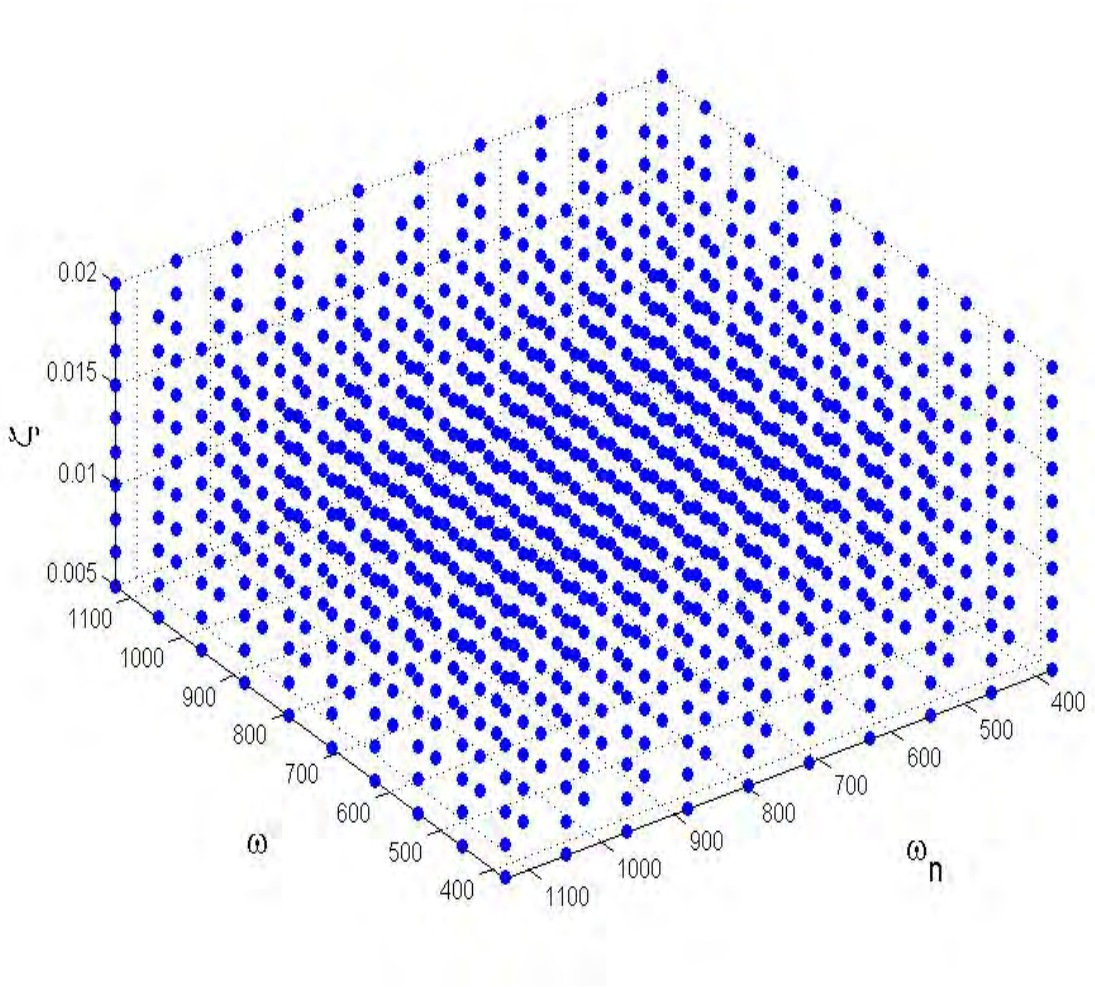

Figure 4.1: m^k factorial sampling.

Figure 4.2 visually depicts the 512 nearly orthogonal and balanced Latin hypercube design points evaluated for the three-variable model.

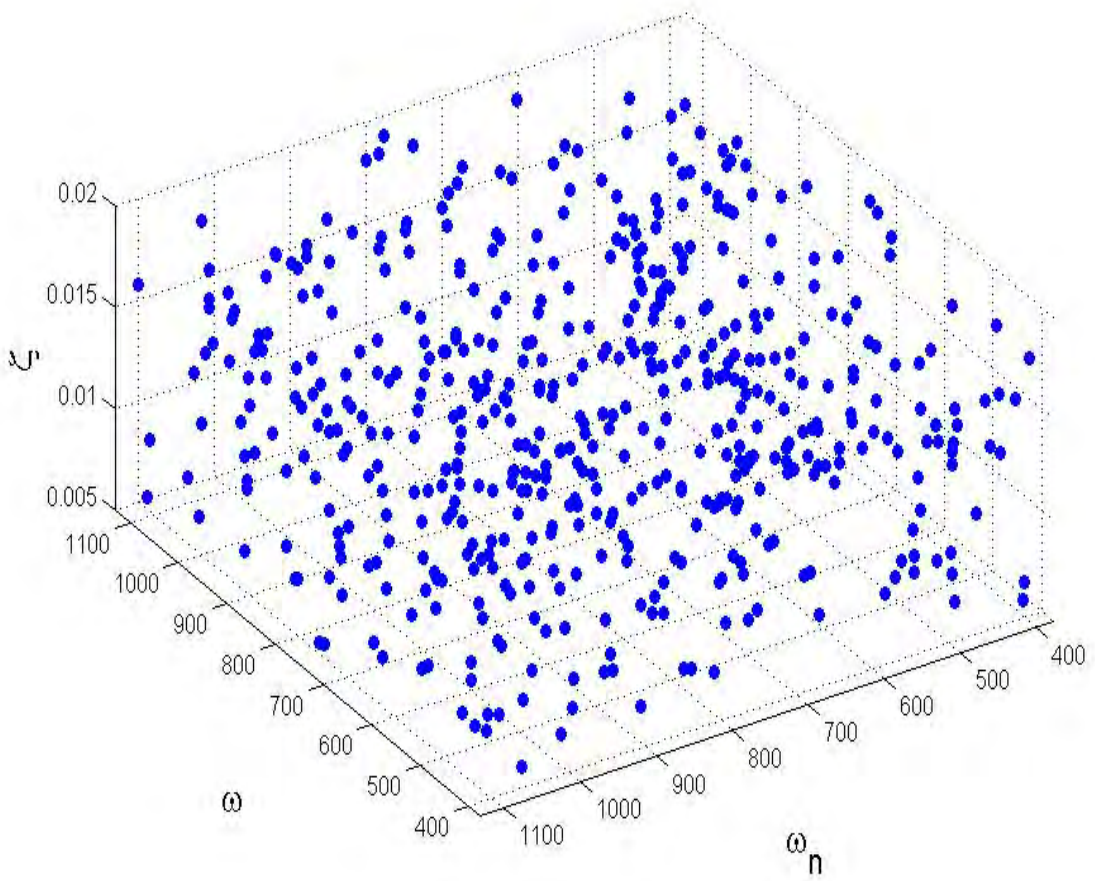

Figure 4.2: Nearly orthogonal and balanced Latin hypercube sampling.

As the reader will notice, the NOBLH sampling method samples extremely well from the interior of the design space and does a poor job sampling from the exterior of the design space. The m^k factorial sampling method, on the other hand, samples uniformly across the design space.

4.8 Sampling Metric: Efficiency

After evaluating all design points in our model, we determine the maximum power generated and determine an optimal combination of factor levels. This m^k factorial method to evaluate the six-variable model is easily accomplished using the MATLAB code referenced in Appendix, Section A.6.

The six-variable power generation model requires 49 floating point operations (flops) in order to compute one design point. The MATLAB code in Appendix, Section A.6 evaluates the power generated for all combinations of the six factors at a varying number of levels. This equates to m^6 design points. Therefore the efficiency of the algorithm with the given number of factors and levels is $49 \times m^6$ flops. This model only consists of six factors and therefore the number of design points required does not change as dramatically with an increase of levels as a model with more factors. For this paper, we use as many as 15 levels per factor. When evaluating the model with 15 levels per factor, $15^6 = 11,390,625$ design points, and $49 \times 11,390,625 \approx 558$ million flops, our Core i7 equipped computer can carry out the algorithm in just over two minutes.

If our model consisted of ten factors, an m^k factorial sampling of 15 levels would consist of $15^{10} \approx 5.77 \times 10^{11}$ design points and too many flops for a standard desk top computer to execute in a week. This algorithm and m^k factorial design are not a wise use of time for simulations with a large number of factors, especially if we desire to change the any aspect of the factors or levels and reproduce the simulation.

The real benefit of nearly orthogonal and balanced Latin hypercube design is its efficiency. Using Vieira's NOB design it is possible to evaluate a model of up to 20 k-level discrete factors (where $k = 2,3...11$ levels) and 100 continuous factors using only 512 design points [30]. Many models or simulations contain many more factors and computations. NOB designs choose very good samplings to test given the limited number of simulations a system can compute in a given time.

4.9 NOBLH Iterative Method

An additional optimization method involves multiple iterations of sampling the design space and using results to restrict the design space to choose design points. In this pa-

per we refer to this method as the NOBLH Iterative method.

First, we use NOBLH design to choose design points from the original design space set by our variable ranges. Next, we analyze the design point that generate the maximum power output. By studying the values of each variable in the optimal design point, we are able to make educated guesses about how to restrict the variable ranges in order to focus our design space.

With each newly discovered optimal design point we are able to restrict the variable ranges and design space until we reach a maximum power or identify an issue that causes a cease to iterations. The aspiration of this method is to arrive at similar results to that of the more costly m^k factorial sampling method while evaluating fewer design points.

It should be noted, the iterative method we use is not as systematic as other iterative methods. Through the use of our NOBLH iterative method we wish to gain insights into our optimization models and better understand alternative methods to optimization.

CHAPTER 5:
Optimization Results and Analysis

5.1 Three-Variable Model NOBLH and m^k Factorial Results

After sampling our design space using both NOBLH and m^k factorial sampling methods we use the resulting design points to find the optimal values of the three variables (ω, ω_n, and ζ) in order to maximize power generation. For the m^k factorial samplings we use levels of 10 and 100. See the Appendix for the Three-Variable Model Optimization Codes for factorial sampling (Section A.4) and NOBLH sampling (Section A.5). The results of each sampling method are summarized in Table 5.1.

Table 5.1: Optimization of power in the three-variable model.

Sampling Method	Design Points	Optimal Power	ω	ω_n	ζ
NOBLH	512	2.49×10^{10}	339.8π	339.8π	0.0122
m^k ($m = 10$)	1,000	7.23×10^{10}	360π	360π	0.005
m^k ($m = 100$)	1,000,000	7.23×10^{10}	360π	360π	0.005

The reader will notice both m^k factorial sampling methods are able to find an optimal power close to three times larger than the NOBLH sampling method. The reader will also notice both m^k factorial samplings determine the optimal values of each factor to be at the extreme of the factors' ranges. The optimal values of ω and ω_n are the maximum values allowed by the range, 360π, and the optimal value of ζ is the minimum value allowed by the range, 0.005. As noted in Chapter 4, the NOBLH sampling fails to adequately sample the extremes of the design space, while the m^k factorial method samples the entire design space uniformly.

This failure of sampling design points in the extremities of the design space accounts for only part of the discrepancy of optimal solutions discovered by the sampling techniques. Notice $\omega = \omega_n$ for both optimal values for the m^k factorial samplings and the NOBLH sampling. After further investigation into the model, we find the optimal values for the ω

and ω_n are always equal.

We can prove this mathematically by analyzing Equation (4.1). In order to maximize the model we obviously want to make the numerator as large as possible while making the denominator as small as possible. In order to eliminate the first part of the denominator, $(1-\frac{\omega^2}{\omega_n^2})^2$, we set $\omega = \omega_n$. This reduces the model to the following equation:

$$\frac{P}{mY_0^2} = \frac{\zeta\omega^3}{4\zeta^2} = \frac{\omega^3}{4\zeta}. \tag{5.1}$$

The three-variable model reduces to a two-variable model in which $\omega = \omega_n$. In order to maximize power, one simply maximizes ω and minimizes ζ.

After analyzing the design points, we discover that, out of the 512 design points in the NOBLH sampling, only four design points set $\omega = \omega_n$, compared to 100 and 1000 points for the $m = 10$ and $m = 100$ m^k factorial samplings, respectively.

Setting $\omega = \omega_n$ plays a crucial role in optimizing this model. The $m = 10$ m^k factorial design selects 100 design points with $\omega = \omega_n$. Out of the said 100 design points, 16 design points produce power greater than the maximum power generated by any of the 512 NOBLH design points. See Figure 5.1 for the sixteen m^k factorial design points that outperform the NOBLH sampling.

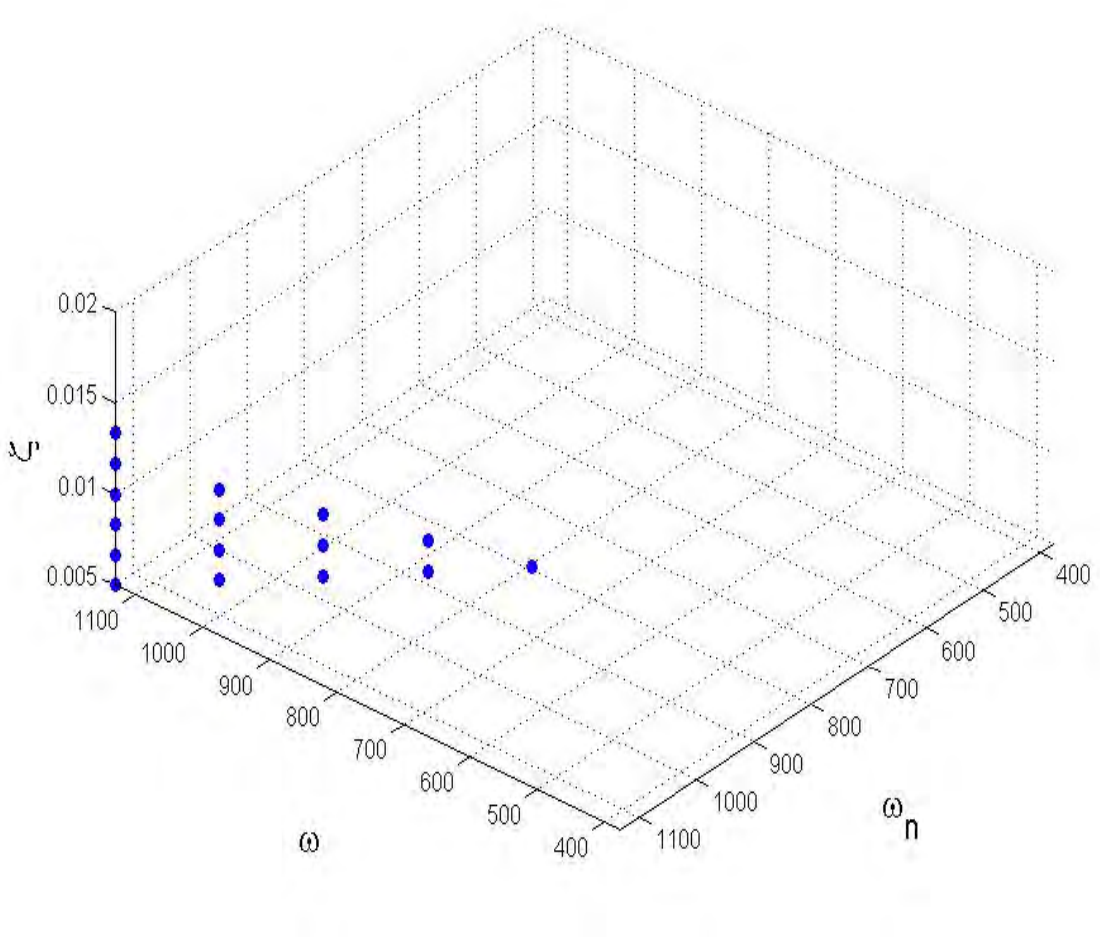

Figure 5.1: m^k factorial design points achieving higher power generation than all NOBLH design points.

While optimizing this particular model, m^k factorial sampling proves the best sampling method. After analysis, we determine that to maximize power one can set $\omega = \omega_n$ and minimize ζ.

5.2 Three-Variable Model NOBLH Iterative Results

After determining the optimal power generation and associated variable values for the three-variable model through the m^k factorial results, we attempt to replicate the results using the NOBLH iterative method. Our initial hopes are the NOBLH iterative method would be able to reach similar results while evaluating less design points than the more costly m^k factorial sampling method. In this particular case, the three level m^k factorial sampling finds the optimal power using only 1000 design points. Even if the NOBLH iterative method finds the optimal results in two iterations, the method would use
$512 \times 2 = 1,024$ design points to do so.

The first iteration of the NOBLH iterative method is identical to the NOBLH sampling method. Table 5.2 uses the same variable ranges as in Table 4.1 and Table 5.3 arrives at the same results as in Table 5.1.

Table 5.2: Iteration one NOBLH iterative variable ranges.

	ω	ω_n	ζ
Lower Limit	120π	120π	0.005
Upper Limit	360π	360π	0.02

Table 5.3: Iteration one NOBLH iterative results.

Optimal Power	ω	ω_n	ζ
2.49×10^{10}	339.8π	339.8π	0.01222

After analyzing the results listed in Table 5.3, we are able to restrain the ranges of ω, ω_n and ζ, listed in Table 5.4. Using the new variable ranges we produce 512 new design points using NOBLH sampling. After evaluating the new design points, we determine the resulting optimal power generation and associated variable values, as shown in Table 5.5.

Table 5.4: Iteration two NOBLH iterative variable ranges.

	ω	ω_n	ζ
Lower Limit	318.3π	318.3π	0.005
Upper Limit	360π	360π	0.015

Table 5.5: Iteration two NOBLH iterative results.

Optimal Power	ω	ω_n	ζ
5.38×10^{10}	349.2π	349.9π	0.0055

Analyzing the results in Table 5.5, we see optimal power increase again along with both values of ω and ω_n. The optimal value of ζ continues to decrease. We use this data to further tighten all variable ranges for the third iteration, listed in Table 5.6.

Table 5.6: Iteration three NOBLH iterative variable ranges.

	ω	ω_n	ζ
Lower Limit	340.6π	340.6π	0.005
Upper Limit	360π	360π	0.006

Table 5.7: Iteration three NOBLH iterative results.

Optimal Power	ω	ω_n	ζ
6.73×10^{10}	357.1π	357.4π	0.005135

Table 5.7 displays an additional increase in optimal power, ω, and ω_n. Additionally, the optimal value of ζ continues to decrease. We are able to restrain the ranges for all variables for the fourth iteration, as listed in Table 5.8.

Table 5.8: Iteration four NOBLH iterative variable ranges.

	ω	ω_n	ζ
Lower Limit	353.3π	353.3π	0.005
Upper Limit	360π	360π	0.0052

Table 5.9: Iteration four NOBLH iterative results.

Optimal Power	ω	ω_n	ζ
7.12×10^{10}	359.4π	359.5π	0.005029

Table 5.9 displays optimal power close to the results found using m^k factorial sampling. After analysis, we further restrain variable ranges for the fifth iteration, listed in Table 5.10.

Table 5.10: Iteration five NOBLH iterative variable ranges.

	ω	ω_n	ζ
Lower Limit	359π	359π	0.005
Upper Limit	360π	360π	0.0052

Table 5.11: Iteration five NOBLH iterative results.

Optimal Power	ω	ω_n	ζ
7.23×10^{10}	360π	360π	0.005002

After five iterations we find optimal power and associated variable values (listed in Table 5.11) equivalent to m^k factorial results. Our conservative methodology to iterative range restriction forces us to reach our results after analyzing $5 \times 512 = 2,560$ design points. The three level m^k factorial sampling optimization method determines the same results after computing only 1000 design points. However, the NOBLH iterative method shows great potential when dealing with a large number of factors.

5.3 Six-Variable Model NOBLH and m^k Factorial Results

After sampling our design space using both NOBLH and m^k factorial sampling methods, we use the resulting design points to find the optimal values of the six variables (A, R, ω_{base}, C_0, w_{SC} and ζ) in order to maximize power generation. For m^k factorial samplings we use levels of 3, 5, 7, 10, 11, and 12. See the Appendix for the Six-Variable Model Optimization Codes for factorial sampling (Section A.6) and NOBLH sampling (Section A.7). The results of each sampling method are given in Table 5.12.

Table 5.12: Optimization of power in the six-variable model.

Method	Design Points	Optimal Power	A	R	ω_{base}	C_0	w_{SC}	ζ
NOBLH	512	7.8509×10^9	0.754	13.129	342.61π	4.1×10^{-8}	344.96π	0.006
m^k ($m = 3$)	729	1.8082×10^{10}	0.5	50.01	360π	1×10^{-6}	360π	0.005
m^k ($m = 5$)	15,625	1.8082×10^{10}	0.5	50.01	360π	1×10^{-6}	360π	0.005
m^k ($m = 7$)	117,649	1.8256×10^{10}	0.337	100	360π	1×10^{-6}	360π	0.005
m^k ($m = 10$)	1,000,000	1.8256×10^{10}	0.337	100	360π	1×10^{-6}	360π	0.005
m^k ($m = 11$)	1,771,561	1.8168×10^{10}	0.402	70.01	360π	1×10^{-6}	360π	0.005
m^k ($m = 12$)	2,985,984	1.8203×10^{10}	0.356	90.91	360π	1×10^{-6}	360π	0.005

Like the three-variable model, all m^k factorial samplings discover combinations of factor values capable of generating power more than twice the value of the NOBLH sampling's optimal solution. Also like the three-variable model, the optimal solution in the m^k factorial samplings includes four variables at the extremes of their ranges. The optimal values of ω_{base}, C_0, and w_{SC} are the maximums of the their ranges, while the optimal value for ζ is the minimum of its range. As we noted in the previous section, NOBLH sampling fails to sample the extremes of the design space. The simulations using the NOBLH design points does not have the opportunity to explore power generation at the extremes of the design space. With only 217 more design points than the NOBLH sampling, the three level m^k factorial sampling creates design points in the extremes of the variable ranges and finds an optimal solution more than twice the value of the NOBLH design solution.

An interesting result of our simulation is that creating a finer grid (increasing the number of levels and resulting design points) does not always result in a more optimal solution. For example, both the $m = 7$ and $m = 10$ m^k factorial samplings find an optimal solution of 1.8256×10^{10}. However, when the number of levels increases from ten to eleven the optimal solution decreases to 1.82168×10^{10}. Additionally, the reader will notice the maximum power found with $m = 12$ sampling is also less than that discovered with $m = 10$ sampling. This can be explained by the fact both the $m = 7$ and $m = 10$ samplings include $A = 0.337$, while the $m = 11$ and $m = 12$ samplings do not.

The true optimal value depends on the precise sampling of A and R. Using the assumption the optimal power generation value occurs at the maximum allowable values of ω_{base}, C_0, and w_{SC} and minimum allowable value of ζ, we are able to further refine the true optimal

values of A and R. We accomplish this refinement by fixing ω_{base}, C_0, w_{SC}, and ζ at their optimal value while sampling 1000 levels each of A and R. This results in refining the optimal values of A as 0.3376 and R as 100. With this more precise value for A we arrive at a new optimal power generation only 6.73×10^4 greater than our previous optimal solution.

5.4 Six-Variable Model NOBLH Iterative Results

After determining the optimal power generation and associated variable values for the six-variable model through the m^k factorial results, we attempt to replicate the results using the NOBLH iterative method. Our aspiration is the NOBLH iterative method will be able to reach similar results while evaluating less design points than the more costly m^k factorial sampling method. From Table 5.12, we see using seven levels the m^k factorial sampling method results with an optimal power of 1.8256×10^{10} after evaluating 117,649 design points. We deem the NOBLH iterative method a success if we reach a optimal power close to the seven level m^k factorial sampling method results with far fewer design points evaluated.

The first iteration of the NOBLH iterative method is identical to the NOBLH sampling method. Table 5.13 uses the same variable ranges as in Table 4.2, and Table 5.14 arrives at the same results as in Table 5.12.

Table 5.13: Iteration one NOBLH iterative variable ranges.

	A	R	ω_{base}	C_0	w_{SC}	ζ
Lower Limit	0.01	0.02	120π	1×10^{-8}	120π	0.005
Upper Limit	0.99	100	360π	1×10^{-6}	360π	0.02

Table 5.14: Iteration one NOBLH iterative results.

Optimal Power	A	R	ω_{base}	C_0	w_{SC}	ζ
7.85×10^9	0.754	13.129	342.6π	4.1×10^{-8}	345π	0.005998

After analyzing the results listed in Table 5.14, we are able to assume optimal power increases when A, R, ω_{base} and w_{SC} take on values closer to their upper most range value. We also assume ζ and C_0 taking values closer to their minimum allowable values results in an increase in power. From these assumptions we tighten the ranges of all three variables,

listed in Table 5.15. Using the new variable ranges we produce 512 new design points using NOBLH design. After evaluating the new design points we determine the resulting optimal power generation and associated variable values, given in Table 5.16.

Table 5.15: Iteration two NOBLH iterative variable ranges.

	A	R	ω_{base}	C_0	w_{SC}	ζ
Lower Limit	0.25	1	340π	1×10^{-8}	340π	0.005
Upper Limit	0.99	100	360π	1×10^{-7}	360π	0.01

Table 5.16: Iteration two NOBLH iterative results.

Optimal Power	A	R	ω_{base}	C_0	w_{SC}	ζ
1.64×10^{10}	0.812	13.98	358.5π	1.28×10^{-8}	358.7π	0.00533

After the second iteration we notice an increase in optimal power, ω_{base}, and w_{SC}. The optimal A and R increase slightly. The optimal ζ and C_0 reduce slightly. Using these findings we further restrain variable ranges, listed in Table 5.17. Our results are shown in Table 5.18.

Table 5.17: Iteration three NOBLH iterative variable ranges.

	A	R	ω_{base}	C_0	w_{SC}	ζ
Lower Limit	0.5	5	358π	1×10^{-8}	358π	0.005
Upper Limit	0.99	50	360π	5×10^{-8}	360π	0.006

Table 5.18: Iteration three NOBLH iterative results.

Optimal Power	A	R	ω_{base}	C_0	w_{SC}	ζ
1.778×10^{10}	0.626	28.24	358.4π	4.1×10^{-8}	358.2π	0.005006

From the third iteration we notice an increased optimal power along with a slight decrease in the optimal values of ω_{base}, w_{SC}, and ζ. The optimal values of A, R, and C_0 increase slightly. We continue restricting variable ranges, listed in Table 5.19.

Table 5.19: Iteration four NOBLH iterative variable ranges.

	A	R	ω_{base}	C_0	w_{SC}	ζ
Lower Limit	0.5	20	358π	2×10^{-8}	358π	0.005
Upper Limit	0.8	30	359π	5×10^{-8}	359π	0.00501

Table 5.20: Iteration four NOBLH iterative results.

Optimal Power	A	R	ω_{base}	C_0	w_{SC}	ζ
1.792×10^{10}	0.728	21.31	358.9π	2.9×10^{-8}	358.9π	0.005

From the results of the fourth iteration, Table 5.20, we see another increase in optimal power. However, knowing the optimal values discovered from m^k factorial sampling, we have made incorrect assumptions restricting the ranges of A, R, ω_{base}, C_0, and w_{SC}. If we further restrict the variable ranges in subsequent iterations we would fail to reach an optimal power similar to that found through m^k factorial sampling.

An alternative way to look at the NOBLH iterative results is purely in terms of the number of design points evaluated. After four iterations, we only evaluate $4\times512=2048$ design points. The optimal power resulting from the NOBLH iterative method (1.792×10^{10}) only represents a 1.84% loss in power from the seven level m^k factorial sampling method (1.8256×10^{10}). Less than a two percent loss in optimal power seems minor when you consider the seven level m^k factorial sampling method requires the evaluation of 117,649 design points. Again, the NOBLH iterative method shows potential when optimizing models with a large number of variables.

5.5 Robustness Analysis

The sampling methods provides the means to find the optimal combination of variable values to maximize power generation in our models. After running simulations with the sampled design points we find the optimal solution for each model. On paper, we then possess the exact metrics to build a piezoelectric generator prototype in order to provide optimal power output. However, the precision of the variable values we insist on paper are not always possible to replicate in experiments or practical application, even under perfect conditions. All variables depending on materials or conditions have associated

variability. For example, a resistor may be advertised as providing a certain number of ohms of resistance, but in reality, provides the advertised ohms of resistance plus or minus some level of discrepancy allowed by the manufacturer.

The purpose of robust design, as a process of simulation optimization, is to identify the "best" solution as one not overly sensitive to small changes in system inputs. In this section we will attempt to identify which factors in the design of a piezoelectric generator need more precision and which factors will allow more variability while producing as much power as possible [32].

5.5.1 Three-Variable Model

Using mathematical models to simulate a real world problem, it is easy to see the variables only as their numerical values. In reality the variables respond to specifications of the piezoelectric generator and its environmental setting.

In this simple three-variable model, engineers will be able to control all of the variables in experimentation. They will be able to set the frequency of excitation (ω) by adjusting the environmental conditions affecting the piezoelectric generator. Additionally, they will be able to set the natural frequency (ω_n) and modal damping ratio (ζ) of the generator by adjusting the design of the prototype.

In the practical application of a piezoelectric generator, certain conditions may not be as easy to control. A piezoelectric generator designed to operate using the vibrations of an air conditioning vent will not be able to depend on a precise or consistent frequency of excitation. Engineers must design the generator to operate within a range of frequency while producing the necessary power.

Earlier in this chapter, we determined that the optimal solution to the three-variable model occurred when $\omega = \omega_n$. Given the fact the environment determines the frequency of excitation, we fixed ω during the robustness analysis while varying ω_n and ζ.

Single Variable Manipulation

We have determined the optimal solution of the three-variable model depends on minimizing ζ while maximizing ω and setting $\omega = \omega_n$. Due to this knowledge we evaluate the

robustness of the optimal solution to the three-variable model in terms of varying ζ and varying the difference between ω and ω_n.

First, we set $\omega = \omega_n = 360\pi$ and vary ζ in order to evaluate the power lost while deviating from the optimal value of ζ. See the results listed in Table 5.21.

Table 5.21: Single variable manipulation of ζ.

ζ	% change in ζ	Power	% Loss
0.005	baseline	7.23×10^{10}	baseline
0.00505	1%	7.162×10^{10}	0.99%
0.00525	5%	6.889×10^{10}	4.76%
0.0055	10%	6.576×10^{10}	9.09%
0.006	20%	6.028×10^{10}	16.67%
0.01	100%	3.617×10^{10}	50%
0.02	300%	1.808×10^{10}	74.75%

A 1%, 5%, or 10% change in ζ results in power losses of less than 10%. A change as drastic as doubling the desired value of ζ results in only a 50% loss in power.

Next, we set $\zeta = 0.005$, $\omega = 360\pi$ and vary ω_n to evaluate the resulting power lost. See the results in Table 5.22.

Table 5.22: Single variable manipulation of ω_n.

ω_n	% change in ω_n	Power	% Loss
360π	baseline	7.23×10^{10}	baseline
360.36π	0.1%	6.948×10^{10}	3.94%
359.64π	-0.1%	6.962×10^{10}	3.75%
360.9π	0.25%	5.775×10^{10}	20.16%
359.1π	-0.25%	5.798×10^{10}	19.84%
361.8π	0.5%	3.608×10^{10}	50.12%
358.2π	-0.5%	3.626×10^{10}	49.87%
363.6π	1%	1.444×10^{10}	80.04%
356.4π	-1%	1.449×10^{10}	79.96%
378π	5%	7.154×10^{8}	99.01%
342π	-5%	7.160×10^{8}	99.01%

The reader will notice the drastic power loss when the separation between ω and ω_n increases. We find that even a 1% discrepancy between ω and ω_n results in a power loss greater than a 300% change in ζ from its optimal value. Whether the ω_n is greater than or less than ω does not make a difference.

Another way to visualize the sensitivity of ω_n and ζ is to plot the resulting power in terms of optimal power as each variable deviates from its optimal value. See Figure 5.2 below.

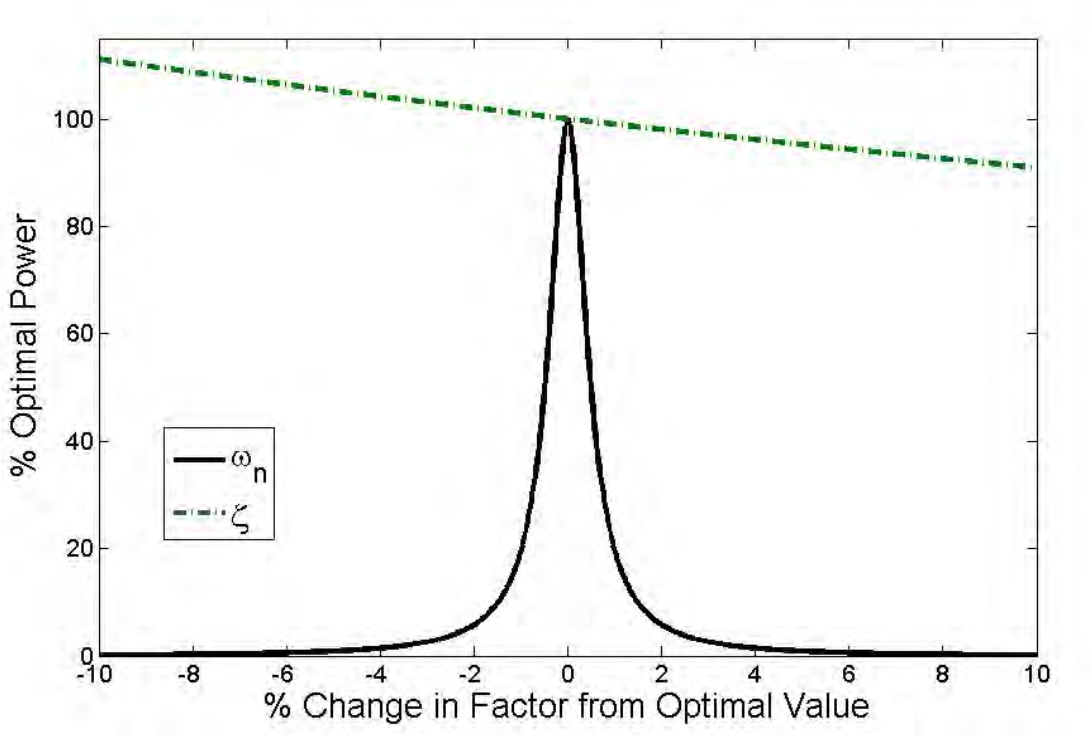

Figure 5.2: Single variable manipulation and resulting percent optimal power.

As seen in Figure 5.2, the reduction of power when ζ increases from its optimal value is linear, with a relatively small slope. On the other hand, when ω_n increases, resulting in an increase in the distance between ω and ω_n, power drastically reduces within the first percentages of change in ω_n.

Alternatively, as ζ decreases from its optimal value, power increases linearly with the same small slope. The reader should note, reducing ζ from its optimal value sets ζ's value outside the values originally studied in this paper. As ω_n decreases from its optimal value, resulting in an increase in the distance between ω and ω_n, power drastically reduces symmetrically to the power reduction resulting from an increase in ω_n from its optimal value.

Upon completion of the single variable manipulation robustness analysis of the three-variable model, we determine the importance of minimizing the discrepancy between ω and ω_n. ζ should be set as low as possible, but the precision of setting ζ should be a second priority to precisely matching ω to ω_n.

Multiple Variable Manipulation

Single variable manipulation provides insight into how the departure from the optimal value of each variable affects power output when the other variables are fixed at their optimal values. While single variable manipulation provides valuable analysis, it is seldom realistic to assume fixing variable values in practical application. A more realistic analysis comprises of treating each variable value as a function of a distribution. The distribution has an upper and lower limit to match the possible limits guaranteed by a manufacture, for example, a capacitor providing 10 ± 1 ohms of resistance. We then analyze how the variable distributions affect the mean and median of power output. From this information we have the ability to make informed recommendations in allowing more or less variability in variable distributions.

We assume that engineers would design the piezoelectric generator in order to optimize power output with a specific frequency of excitation in mind. The generator itself cannot manipulate the environment and accompanying frequency of excitation. To simulate this assumption we set the frequency of excitation, ω, to the optimal value of 360π. We are more interested in finding how the variation in design specifications of the piezoelectric generator affects power output.

In order to guarantee that variable values stayed within desired limits, we use triangle distributions. First, using SAS's commercial statistical discovery software, JMP, we create triangle distributions for both ω_n and ζ with modes equal to their respective optimal values (ω_n=360π, ζ=0.005) and the limits at $\pm$10% the optimal values. Using JMP, we create 10,000 sample points from the distributions and fixed value of ω and computed 10,000 power outputs using the three-variable model. The distributions of ω_n, ζ and the resulting power output are illustrated in Figure 5.3.

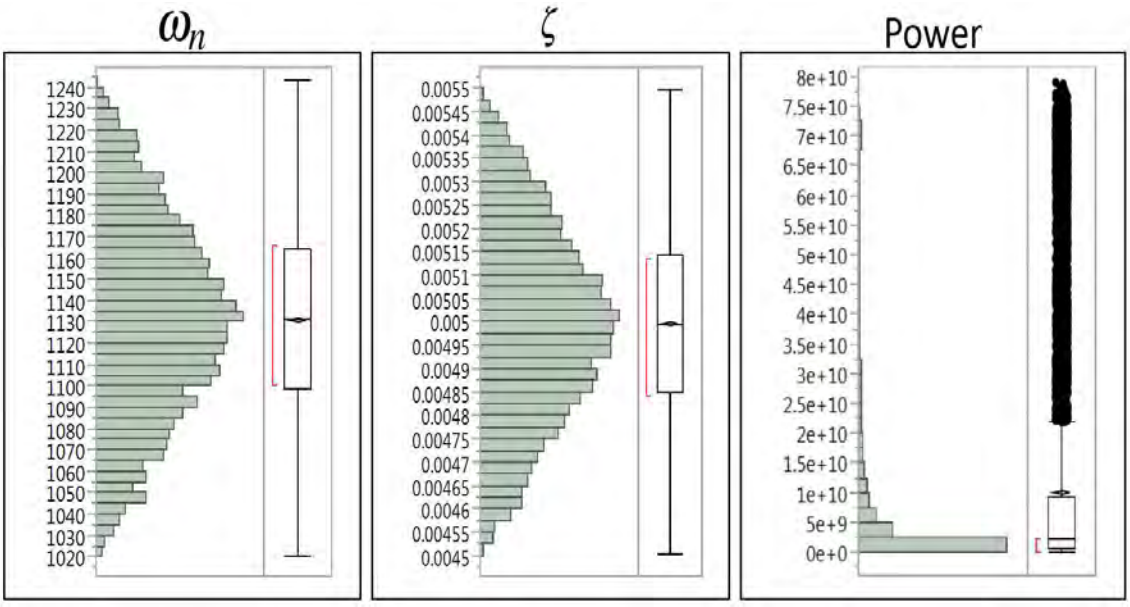

Figure 5.3: $\omega_n \pm 10\%$, $\zeta \pm 10\%$, and resulting power distributions.

Letting ω_n and ζ vary 10% from their optimal values results in a mean power output of 9.976×10^9. This mean power represents an 86% loss from the optimal value. Furthermore, the median power output is only 2.09×10^9, a 97% loss from the optimal power value. This means 50% of all the design points produce a loss of 97% or more.

Next, we use insights derived from the analysis of the single variable manipulation to drive our quest for more power output. We see from single variable manipulation the importance of setting $\omega = \omega_n$ in order to maximize power. In the following distribution we allow ω_n to vary only 5% from its optimal value, while allowing ζ to vary 10%. See Figure 5.4 for the ω_n, ζ, and resulting power distributions.

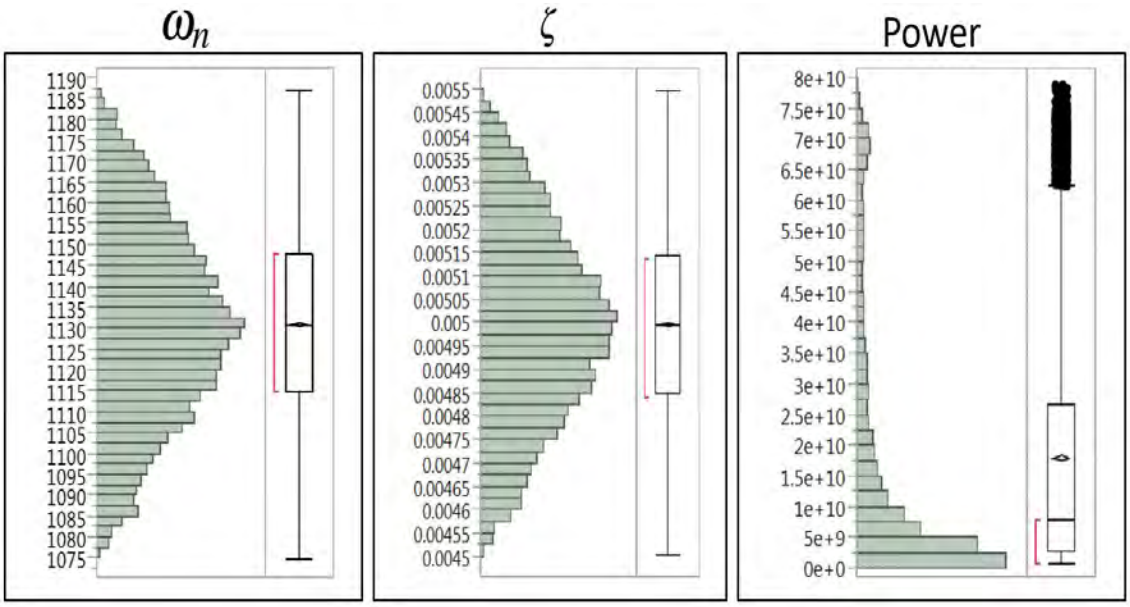

Figure 5.4: $\omega_n \pm 5\%$, $\zeta \pm 10\%$, and resulting power distributions.

Tightening the distribution to allow for only a 5% variation of ω_n while keeping the previously used ζ distribution results in a mean power output of 1.782×10^{10}, a 75% loss from the optimal power value. The resulting median power output for these distributions equals 7.51×10^9, a 90% power loss. Even if the results are not overwhelming, this restriction of variation for ω_n leads to an improvement in power.

Due to the results we see from slightly tightening the ω_n distribution, we decide to investigate further by allowing ω_n to vary only 1% from its optimal value while allowing ζ to continue to vary 10% from optimal. See Figure 5.5 for the ω_n, ζ, and resulting power distributions.

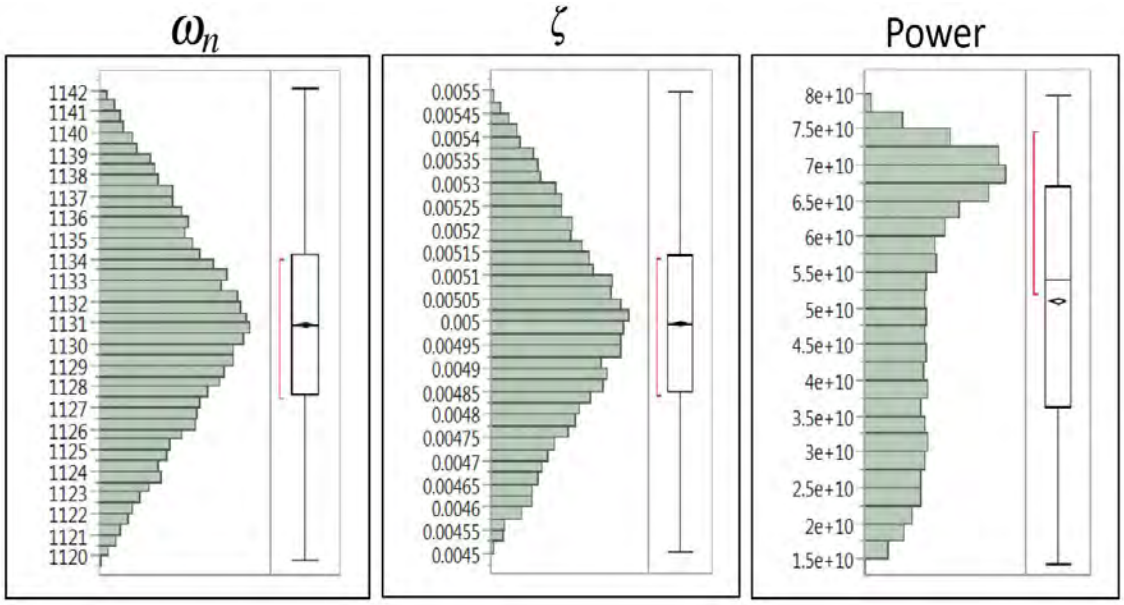

Figure 5.5: $\omega_n \pm 1\%$, $\zeta \pm 10\%$, and resulting power distributions.

Further tightening the distribution to allow for only a 1% variation of ω_n while keeping the previously used ζ distribution results in a mean power output of 5.131×10^{10}, a 29% loss from the optimal power value. The resulting median power output for these distributions equals 5.4×10^{10}, a 25% power loss. This is a drastic improvement in power output. Notice the power distribution's shape changes as well, resulting in an increased likelihood of generating power close to the optimal and shifting the median power output above the mean.

Next, we try to further improve upon our findings by restricting the variation of ζ from its optimal value. We tighten the distribution of ζ to only 5% of its optimal value while keeping ω_n's distribution to allow an deviation of 1% of its optimal value. See Figure 5.6 for the ω_n, ζ, and resulting power distributions.

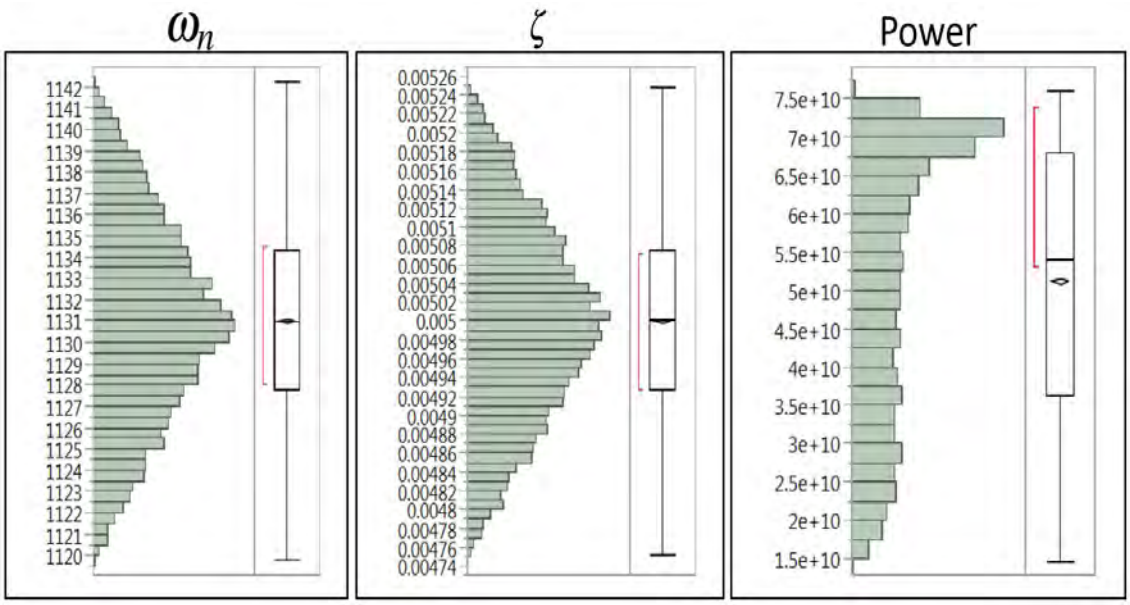

Figure 5.6: $\omega_n \pm 1\%$, $\zeta \pm 5\%$, and resulting power distributions.

Tightening the distribution to allow for only a 5% variation of ζ while keeping the previously used ω_n distribution results in a mean power output of 5.128×10^{10}, a 29% loss from the optimal power value. The resulting median power output for these distributions equals the median of the previous distributions at 5.4×10^{10}, a 25% power loss. We find tightening ζ's distribution actually leads to a decrease in mean power output. This is due to the fact when $\omega = \omega_n$ as ζ approaches zero power increases infinitely. That is, there exists a vertical asymptote when $\zeta = 0$. With a tighter distribution, the value of ζ does not have the ability to take on smaller values.

Using multiple variable manipulation robust analysis we find when attempting to optimize power it is best to allow as little variation as possible from natural frequency's (ω_n) optimal value. This will minimize the discrepancy between ω and ω_n and result in greater power output. The restriction of the variation of the modal damping ration (ζ) from its optimal

value is not as important. In fact, we find if the variation of ζ would allow a smaller value than the desired setting, the model generates even greater power.

5.5.2 Six-Variable Model

In the six-variable model, engineers are able to control all of the variables in experimentation. They are able to set the base motion driving frequency (ω_{base}) by adjusting the environmental conditions affecting the piezoelectric generator. Additionally, they are able to set the electromechanical coupling coefficient (A), load resistance (R), net clamped capacity of piezoelectric material (C_0), modal short circuit net frequency (w_{SC}) and modal damping ratio (ζ) by adjusting the design of the prototype.

In the practical application of a piezoelectric generator certain conditions may not be as easy to control. A piezoelectric generator designed to operate using the vibrations of an air conditioning vent will not be able to depend on a precise or consistent base motion driving frequency. Given the fact the environment determines the base motion driving frequency, we fix ω_{base} during the robustness analysis while varying the other five factors.

Single Variable Manipulation

Earlier in this chapter, we determined the optimal solutions of the six-variable model in order to optimize power. To remind the reader of these values we include Table 5.23.

Table 5.23: Optimal values for each variable in the six-variable model.

Max Power	A	R	ω_{base}	C_0	w_{SC}	ζ
1.8256×10^{10}	0.3376	100	360π	1×10^{-6}	360π	0.005

First, we fix all variables at their optimal values and vary the electromechanical coupling coefficient (A). See the results in Table 5.24.

Table 5.24: Single variable manipulation of A.

A	% change in A	Power	% Loss
0.3376	baseline	1.8256×10^{10}	baseline
0.30384	-10%	1.8057×10^{10}	1.09%
0.32072	-5%	1.8209×10^{10}	0.26%
0.3342	-1%	1.8254×10^{10}	0.01%
0.3410	1%	1.8254×10^{10}	0.01%
0.3545	5%	1.8211×10^{10}	0.25%
0.3714	10%	1.8088×10^{10}	0.92%

From the data presented, it appears varying A does not drastically decrease power output. Varying A by 10% from its optimal value only results in around a 1% loss in power.

Next, we fix all variables at their optimal values and vary load resistance (R). See the results in Table 5.25.

Table 5.25: Single variable manipulation of R.

R	% change in R	Power	% Loss
100	baseline	1.8256×10^{10}	baseline
90	-10%	1.8175×10^{10}	0.44%
95	-5%	1.8228×10^{10}	0.15%
99	-1%	1.8252×10^{10}	0.02%
101	1%	1.8259×10^{10}	-0.02%
105	5%	1.8262×10^{10}	-0.04%
110	10%	1.8251×10^{10}	0.03%

By analyzing the data above we see that varying R changes power by even less than the variation of A. The reader will notice negative loss when R takes on the value of 101 and 105 ohms. This represents a gain of power at those values of R. The reader will also notice increasing R past those values to 110 ohms results in a power loss from the baseline. It is interesting to note, that had we initially included 105 ohms in the range of load resistance to be studied we would find a different optimal value of R.

Next, we fix all variables at their optimal values and vary the net clamped capacity of piezoelectric material (C_0). See the results in Table 5.26.

Table 5.26: Single variable manipulation of C_0.

C_0	% change in C_0	Power	% Loss
1×10^{-6}	baseline	1.8256×10^{10}	baseline
9×10^{-7}	-10%	1.8223×10^{10}	0.18%
9.5×10^{-7}	-5%	1.8239×10^{10}	0.09%
9.9×10^{-7}	-1%	1.8253×10^{10}	0.02%
1.01×10^{-6}	1%	1.8259×10^{10}	-0.02%
1.05×10^{-6}	5%	1.8274×10^{10}	-0.1%
1.1×10^{-6}	10%	1.8292×10^{10}	-0.2%

The variation of C_0 from its optimal value results in small variation of power output. Also, as C_0 increases so does the power. From the results above, we assume if we had included a larger value as the maximum limit of C_0 to study we would derive a larger value of C_0 as its optimal value.

Next we fix all variables at their optimal values and vary the modal short circuit net frequency (w_{SC}). See the results in Table 5.27.

Table 5.27: Single variable manipulation of w_{SC}.

w_{SC}	% change in w_{SC}	Power	% Loss
360π	baseline	1.8256×10^{10}	baseline
324π	-10%	2.0229×10^{8}	98.89%
342π	-5%	7.5408×10^{8}	95.87%
356.4π	-1%	9.7642×10^{9}	46.51%
363.6π	1%	8.5501×10^{9}	53.17%
378π	5%	6.5336×10^{8}	96.42%
396π	10%	1.6194×10^{8}	99.11%

Variation in w_{SC} results in large power loss. As small as a 1% deviation in modal short circuit frequency results in close to a 50% loss in power. A 10% deviation of w_{SC} results in

a 99% power loss. The six-variable model is extremely sensitive to variations of w_{SC} from its optimal value.

As in the three-variable model, the difference between two frequencies in the six-variable model greatly impact power generation. In this robustness study we fix ω_{base} at its optimal value and vary w_{SC}. Due to the fixed ω_{base}, the relationship between the two frequencies and power generation is not obvious to the reader. However, after analyzing Equation (4.1), the reader will notice when $\omega_{base} = w_{SC}$ the denominator decreases by eliminating $(-{\omega_{base}}^2 + {w_{SC}}^2)(1 + {C_0}^2{\omega_{base}}^2R^2)$. The decrease in the denominator of Equation (4.1) leads to greater power generation.

Finally, we fix all variables at their optimal values and vary the modal damping ratio (ζ). See the results in Table 5.28.

Table 5.28: Single variable manipulation of ζ.

ζ	% change in ζ	Power	% Loss
0.005	baseline	1.8256×10^{10}	baseline
0.0045	-10%	2.0227×10^{10}	-10.79%
0.00475	-5%	1.9203×10^{10}	-5.19%
0.00495	-1%	1.8440×10^{10}	-1.01%
0.00505	1%	1.8075×10^{10}	0.99%
0.00525	5%	1.7377×10^{10}	4.82%
0.0055	10%	1.6560×10^{10}	9.29%

The variation of ζ from its optimal value results in small variation of power output. Also, as ζ decreases the power increases. From the results above we could assume that if we had included a smaller value as the minimum limit of ζ to study we would derive a smaller value of ζ as its optimal value, as in Figure 5.7.

Another way to visualize the sensitivity of each variable is to plot the resulting power in terms of optimal power as each variable deviates from its optimal value.

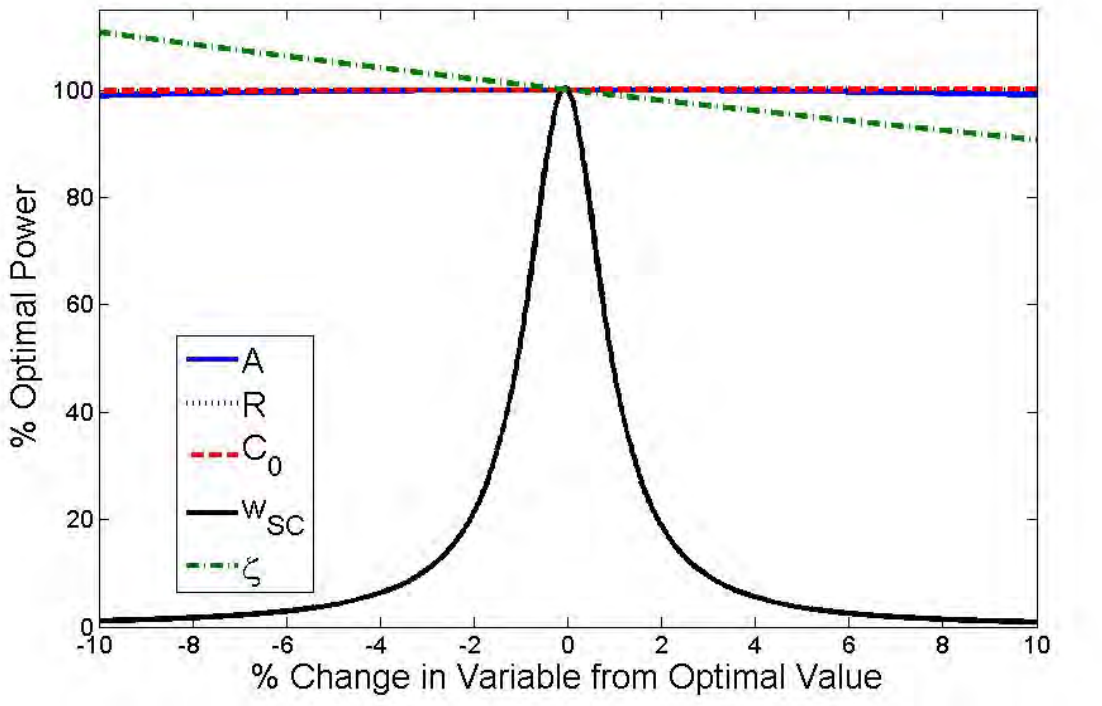

Figure 5.7: Single variable manipulation and resulting percent optimal power.

Figure 5.7 further illustrates the need to set w_{SC} to its precise optimal value. The effects of all other variables are drowned out by w_{SC}'s dominating negative effect. Individually A, R, and C_0 change power output insignificantly even under $\pm 10\%$ deviations from their optimal values. ζ demonstrates its ability to linearly effect power both negatively and positively.

In order to see the effects of the less sensitive variables, see the zoomed in plot in Figure 5.8.

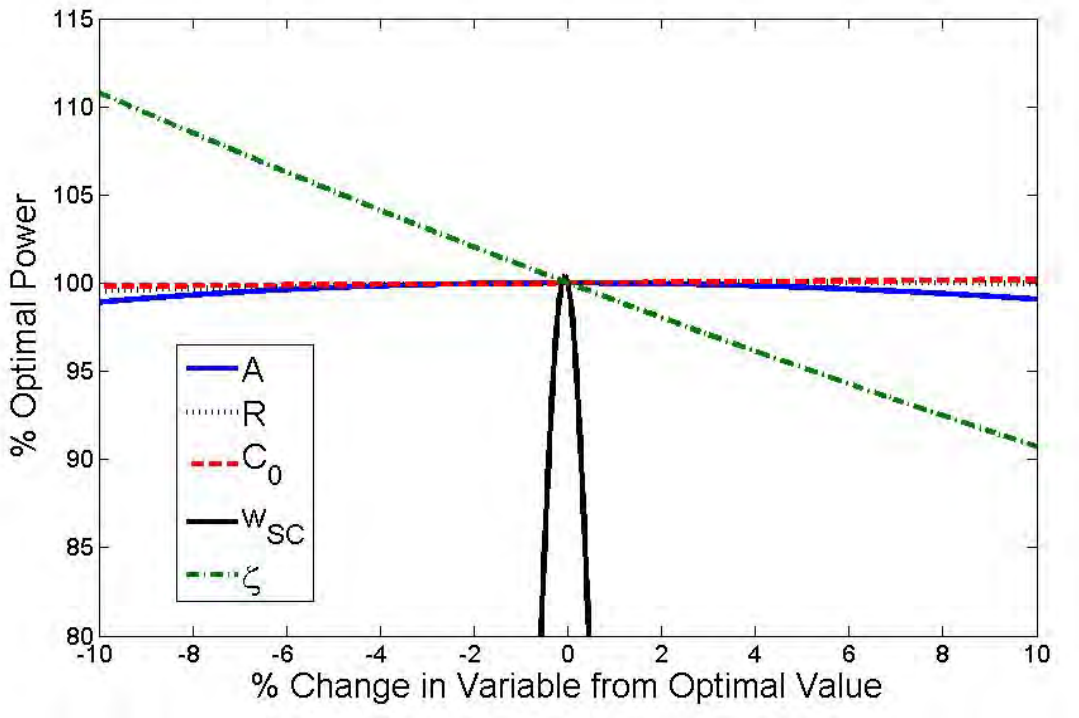

Figure 5.8: Zoomed-in single variable manipulation and resulting percent optimal power.

From Figure 5.8 one will notice, after w_{SC}, the deviations of ζ have the largest impact on power output. Also notice a change of -10% in ζ increases power slightly more than a change of 10% in ζ decreases power.

The zoomed-in plot also illustrates the curvature of A's power curve. The optimal value of A would not have changed even if we selected a wider range of A values to study.

Upon completion of the single variable manipulation of the six-variable model robustness analysis, we find modal short circuit net frequency (w_{SC}) proves by far the most sensitive variable. A deviation of $\pm 10\%$ w_{SC} from its optimal value results in around a 99% power loss. On the opposite end of the spectrum a deviation of $\pm 10\%$ A, R, or C_0 from their optimal values results in a power loss of around 1% or less. Interesting to note, slightly

increasing R or C_0 or decreasing ζ results in a power gain.

Multiple Variable Manipulation

As previously discussed in the three-variable model robustness analysis, the single variable manipulation of the six-variable model provides insight into how the departure from the optimal value of each variable affects power output when the other variables are fixed at their optimal values. Like the three-variable multiple variable robustness analysis we use variable distributions to attempt to identify which variables require more precision and thus less variation from their optimal value in order to maximize power.

We assume that engineers design the piezoelectric generator in order to optimize power output with a specific frequency of excitation in mind. The generator itself cannot manipulate the environment and accompanying frequency of excitation. To simulate this assumption we set the base motion driving frequency, ω_{base}, to the optimal value of 360π. We are more interested in finding how the variation in design specifications of the piezoelectric generator affect power output.

In order to guarantee that variable values stay within desired limits we use triangle distributions. First, using SAS's commercial statistical discovery software, JMP, we create triangle distributions for the five variables in the six-variable model with modes equal to their respective optimal values ($A = 0.3376$, $R = 100$, $C_0 = 1 \times 10^{-6}$, $w_{SC} = 360\pi$, and ζ=0.005) and the limits at $\pm$ 10% the optimal values. Using JMP, we create 10,000 sample points from the distributions and fixed value of ω_{base}, and compute 10,000 power outputs using the six-variable model. See the distributions of the variables and the resulting power output in Figure 5.9.

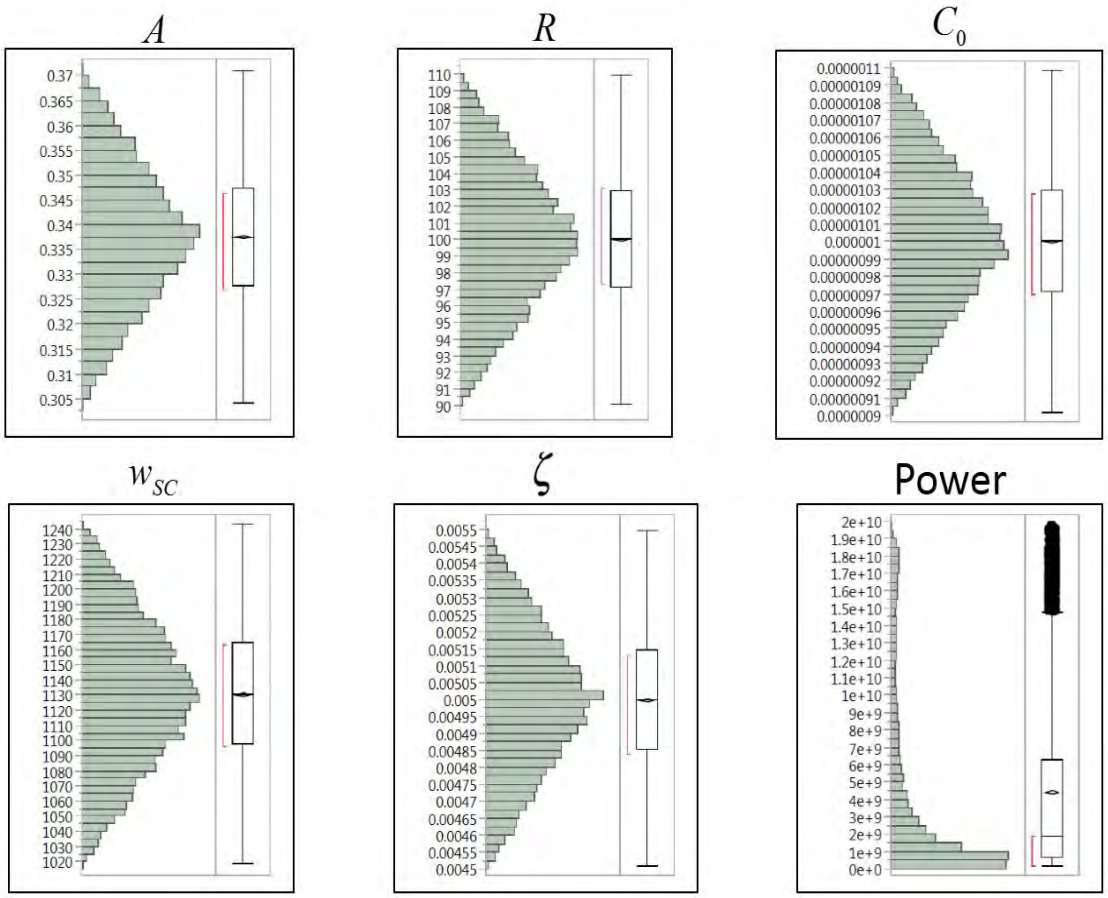

Figure 5.9: $A \pm 10\%$, $R \pm 10\%$, $C_0 \pm 10\%$, $w_{SC} \pm 10\%$, $\zeta \pm 10\%$, and resulting power distributions.

Letting the five variables vary 10% from their optimal values results in a mean power output of 4.4875×10^9. This mean power represents a 75% loss from the optimal value.

Furthermore, the median power output is only 1.92×10^9, an 89% loss from the optimal power value. This means 50% of all the design points produce a loss of 89% or more of the optimal value.

Next, we use insights derived from the analysis of the single variable manipulation to seek more power output. From single variable manipulation we determine w_{SC} to be the most sensitive variable in the six-variable power generation model. In the following distribution we allow w_{SC} to vary only 5% from its optimal value, while allowing the other four variables a 10% variation. See the distributions of the variables and the resulting power output in Figure 5.10.

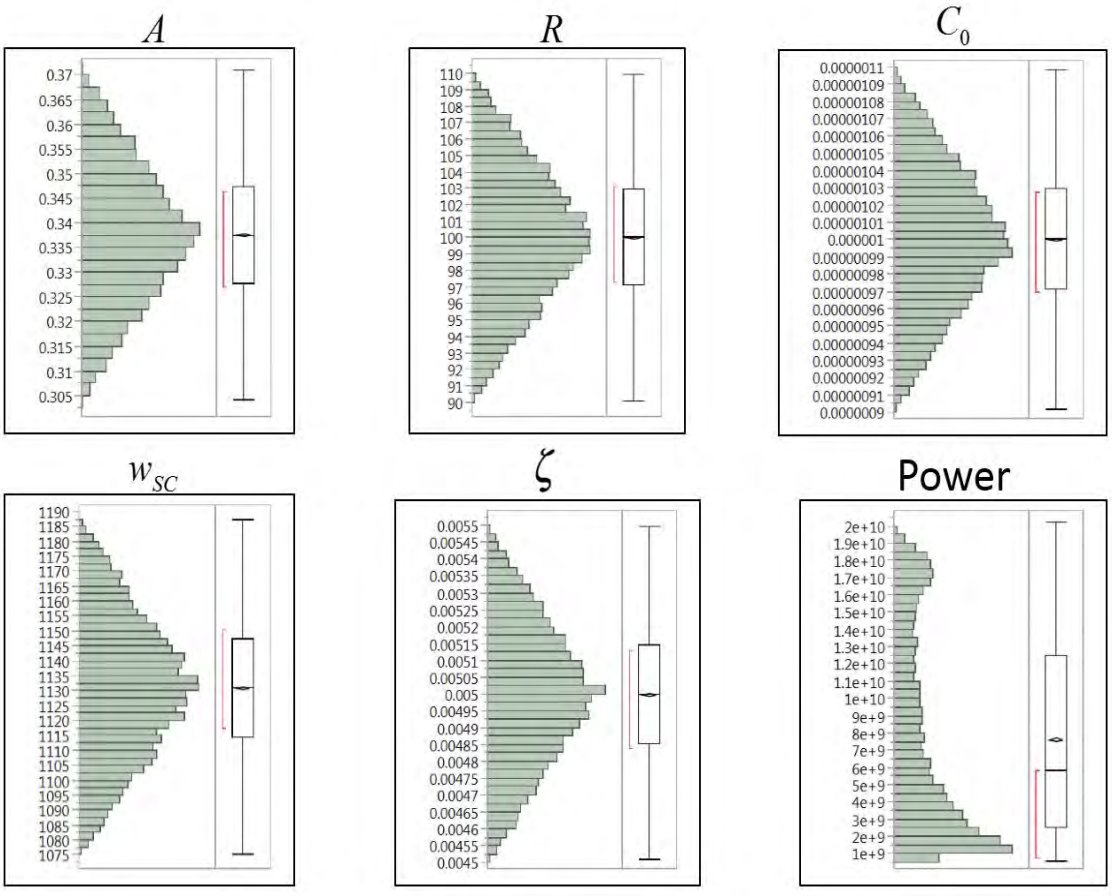

Figure 5.10: $A \pm 10\%$, $R \pm 10\%$, $C_0 \pm 10\%$, $w_{SC} \pm 5\%$, $\zeta \pm 10\%$, and resulting power distributions.

Allowing w_{SC} to vary only 5% from its optimal value while allowing the other four vari-

ables a 10% variation results in a mean power of 7.6514×10^9, representing a 58% power loss. This is a 17% improvement in mean power loss from allowing w_{SC} 10% variability. Additionally, the median power output is 5.8×10^9, a 68% power loss. The median power loss is a 21% improvement over allowing w_{SC} 10% variability.

Figure 5.10 illustrates the benefit of constraining the variation of the modal short circuit net frequency. Next, we further tighten the variation of w_{SC} to 1% while maintaining the other four variables at 10% variation. See the distributions of the variables and the resulting power output in Figure 5.11.

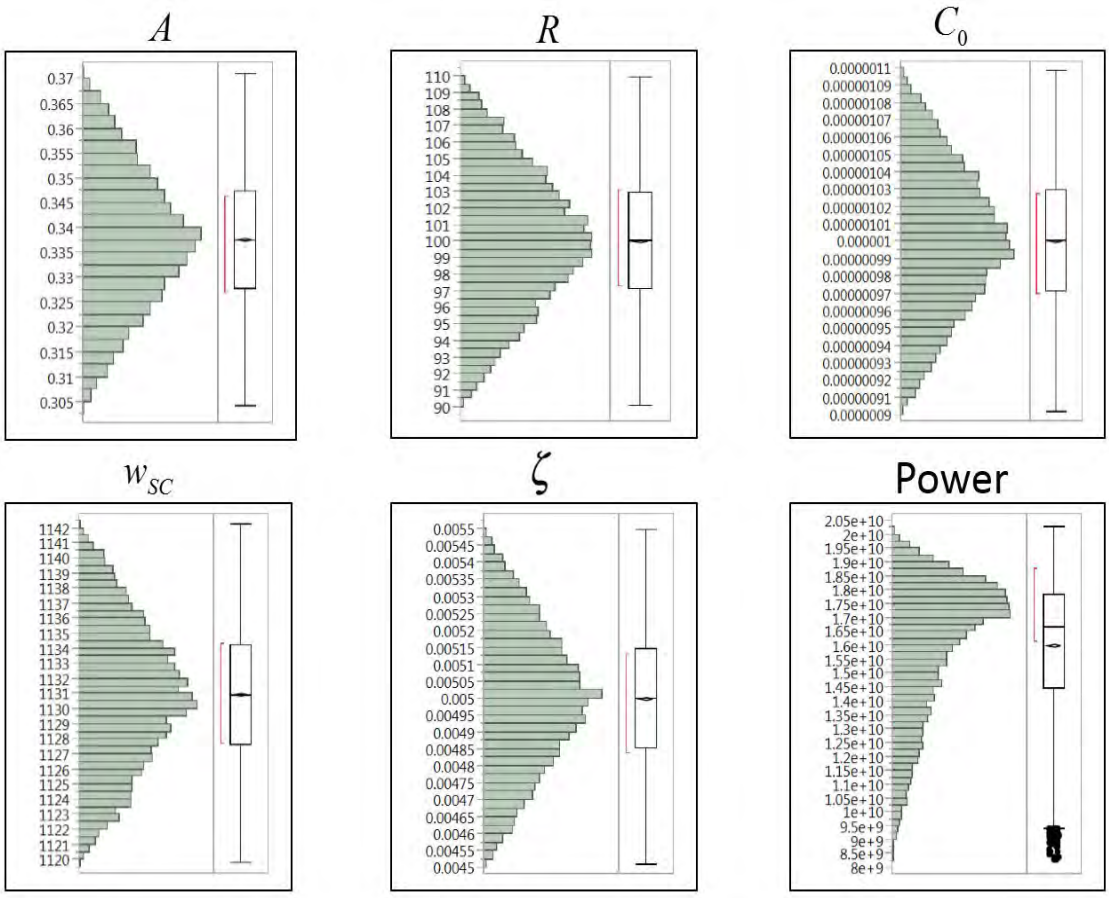

Figure 5.11: $A \pm 10\%$, $R \pm 10\%$, $C_0 \pm 10\%$, $w_{SC} \pm 1\%$, $\zeta \pm 10\%$, and resulting power distributions.

Further tightening the variation of the modal short circuit net frequency results in an even greater mean power output of 1.599×10^{10}, representing only a 12% power loss from the

optimal power. Furthermore, the reader will notice the power distribution changing drastically as well, resulting in a median power greater than the mean power. The median power output is 1.7×10^{10}, a power loss of only 7% from the optimal power.

We learn the importance of minimizing the variation of the modal short circuit frequency from its optimal value. If we cannot guarantee a 1% variation constraint on w_{SC}, is it possible to make up power output by tightening the variation of the other four variables? We attempt to answer the above question by allowing all five variables a 5% variation to compare power output to previous results. See the distributions of the variables and the resulting power output in Figure 5.12.

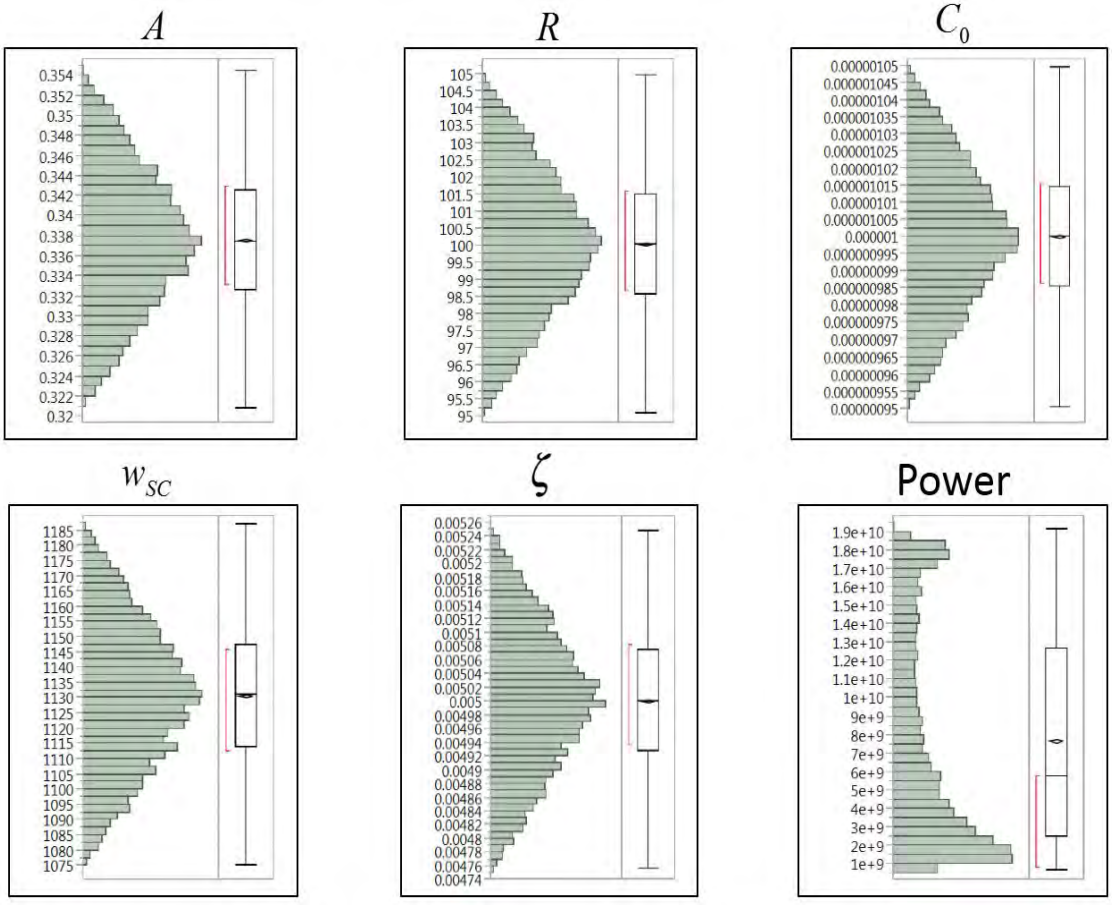

Figure 5.12: $A \pm 5\%$, $R \pm 5\%$, $C_0 \pm 5\%$, $w_{SC} \pm 5\%$, $\zeta \pm 5\%$, and resulting power distributions.

From Figure 5.12 we see a power distribution similar to that of Figure 5.10. In fact, restrict-

ing all variables to a 5% variation results in a mean power of 7.656×10^9, representing a 58% power loss from the optimal power. This mean power is extremely similar to the results displayed in Figure 5.10. Additionally similar to the results from Figure 5.10, the median power output is 5.75×10^9, representing a 69% power loss. We find tightening the variation of the variables other than the modal short circuit net frequency results in negligible power improvement over when we restrict w_{SC} to 5% variation and allow 10% variation for the other four variables.

Our next question asks whether it is possible to generate a best case scenario by restricting all variables to 1% variation. Do we see significant improvement over when we restrict w_{SC} to 1% variation while allowing the four other variables 10% variation? See the distributions of the variables and the resulting power output in Figure 5.13.

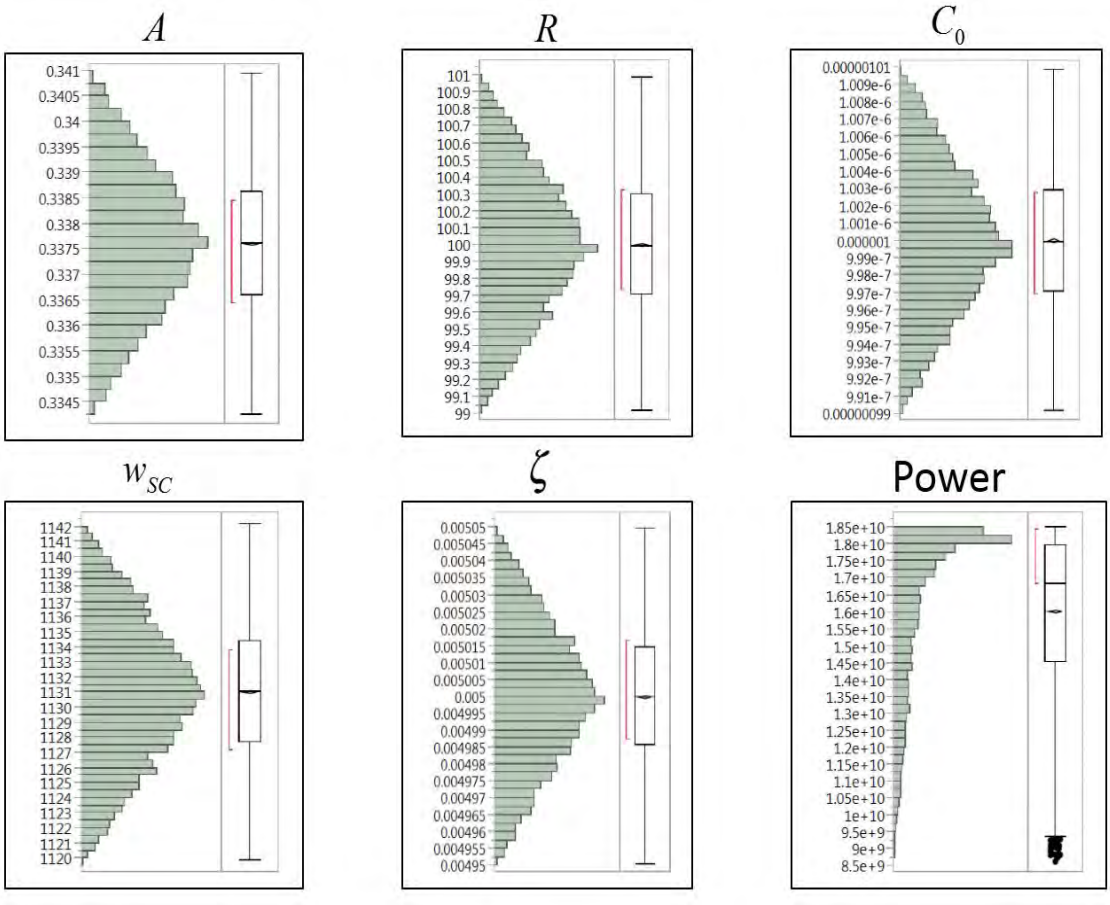

Figure 5.13: $A \pm 1\%$, $R \pm 1\%$, $C_0 \pm 1\%$, $w_{SC} \pm 1\%$, $\zeta \pm 1\%$, and resulting power distributions.

Comparing the power distribution in Figure 5.13 with the power distribution in Figure 5.11, we notice the likelihood of producing power close to the optimal increases. The power distribution in Figure 5.11, however, displays the possibility of producing power greater than the optimal. As we discussed in single variable manipulation, this occurs when ζ is smaller than its optimal value or C_0 or R is greater than its optimal value.

Restraining all variables to a 1% variation results in a mean power of 1.601×10^{10}, representing a 12% power loss, and a median power of 1.7×10^{10}, representing a 7% power loss. The restriction of all variables to a 1% variation results in a negligible benefit in terms of mean and median power compared to restraining modal short circuit net frequency to 1% variation while allowing the other four variables 10% variation.

We see when we tighten the variation of w_{SC} to 1% and allow 10% variation of the other variables there is a possibility of generating power greater than the optimal. During single variable manipulation we determined decreasing ζ from its optimal value has the greatest influence in increasing power. We also note decreasing ζ 10% increases power slightly more than increasing ζ 10% decreases power. Are we able to produce a higher mean and median power if we allow ζ to vary 10% while restricting all other variables to 1% variation? See the distributions of the variables and the resulting power output in Figure 5.14.

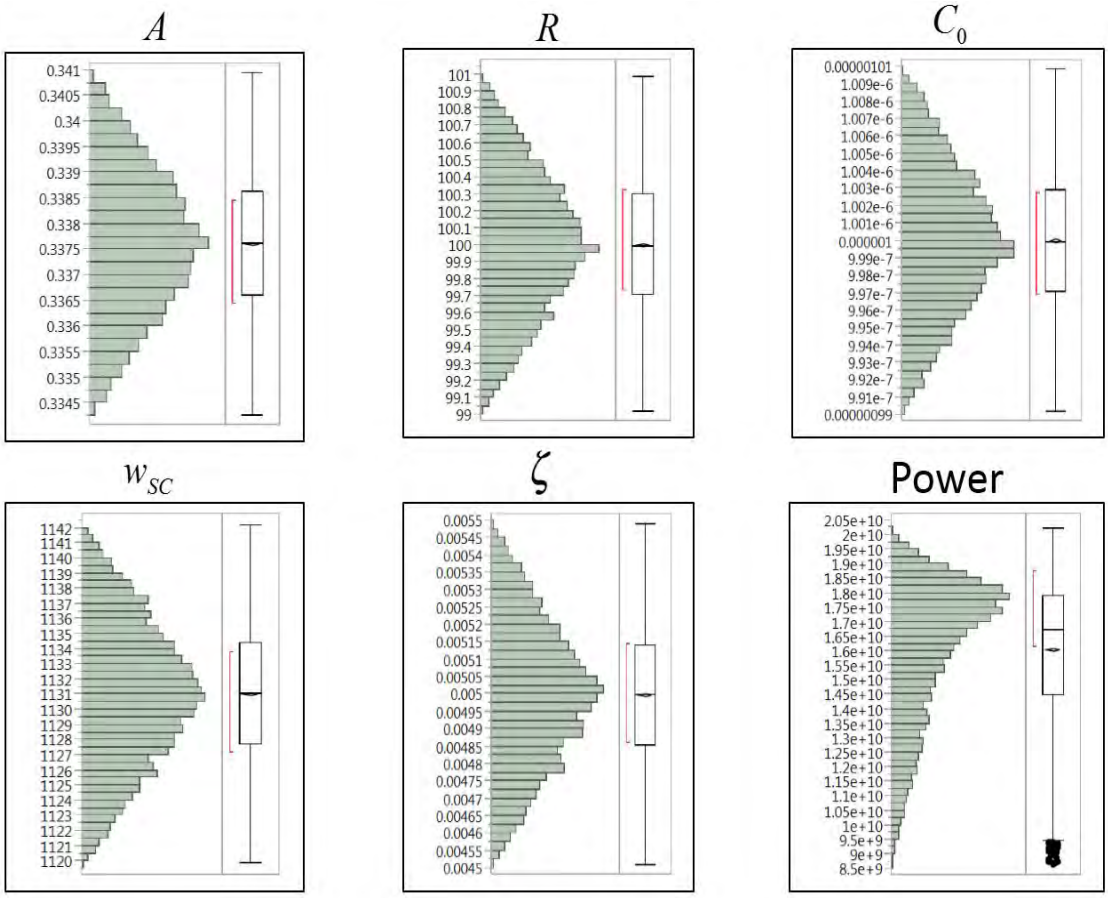

Figure 5.14: $A \pm 1\%$, $R \pm 1\%$, $C_0 \pm 1\%$, $w_{SC} \pm 1\%$, $\zeta \pm 10\%$, and resulting power distributions.

The power distribution in Figure 5.14 looks extremely similar to the power distribution in Figure 5.11 when we restrict w_{SC} to 1% variation while allowing 10% variation for all other variables. For both power distributions there are possibilities of producing power greater than the optimal and a high likelihood of producing power approximate to the optimal. Additionally, the power distributions have extremely similar means and medians. The mean and median power produced for the distribution above are 1.604×10^{10} and 1.7×10^{10}, respectively. This accounts for a mean power loss of 12% and a median power loss of 7%.

Although not an overwhelming front runner, we find that the best mean power results from restricting all variables to 1% variation while allowing ζ 10% variation. This produces a difference of only 3×10^7 greater power than restricting all variables to 1% variation.

The biggest takeaway from the six-variable robustness analysis is the importance in minimizing the variation of the modal short circuit net frequency (w_{SC}) from its optimal value. The restriction of variation for all other variables should be a distant second priority. In fact allowing the modal damping ratio (ζ) to vary from its optimal improves mean power production slightly.

CHAPTER 6:
Conclusion

6.1 Summary of Results

The military is looking for alternative energy sources to provide deployed bases with electricity. Diesel fueled generators and their large logistics tails have proven expensive and a liability to force protection. The alternative energy focus for now is solar, but solar arrays require infrastructure and space. Piezoelectric generators, combined with other renewable energy means, could provide a more efficient means of electricity production to fossil fuel powered generators. Additionally, new methods of energy storage could eventually facilitate alternative energy use in military applications [33].

This paper attempted to find the optimal designs involving material parameters in the piezoelectric generator as well as the generator's environment in order to maximize electric output. Our hope is that the results of this paper will serve as a step towards the practical application of efficient piezoelectric generators and contribute to preserving the combat capability of the US Military. Through the study of two mathematical models we found the optimal values for variables given constrained ranges. We presented the optimal values for the three-variable model in Table 5.1 and the optimal values for the six-variable model in Table 5.12.

6.1.1 Three-Variable Model Analysis

In the detailed analysis of the three-variable model, we study the power as both a function of normalized frequency and a function of modal damping ratio and frequency. When we analyze power as a function of normalized frequency, we find that generating maximum power the optimal normalized frequency ($x = \frac{\omega}{\omega_n}$) depends on the value of the modal damping ratio (ζ). As ζ approaches zero the optimal normalized frequency approaches one. When we analyze power as a function of modal damping ratio and normalized frequency, we are able to visualize the potential power generation capability by minimizing ζ and setting the normalized frequency to one. Finally, we use Roundy and Wright's results [15] to support our simple three-variable model.

6.1.2 Six-Variable Model Analysis

Through the analysis of the six-variable model optimization results we find that power increases as the base motion driving frequency (ω_{base}), net clamped capacity of piezoelectric material (C_0), and modal short circuit net frequency (w_{SC}) increases and modal damping ratio (ζ) decreases. The optimal values for the electromechanical coupling coefficient (A) and load resistance (R) vary depending on sampling method. There appears to be a correlation in power output and the difference of ω_{base} and w_{SC}.

6.1.3 Sampling Methods

In our search for optimal values to maximize power production we use two sampling methods, m^k factorial and nearly orthogonal and balance Latin hypercubes (NOBLH). Although the NOBLH design provides nearly orthogonal samplings with fair space-filling properties, its failure to effectively sample the extremes of the design space leads to less than optimal results. In both of our models, the optimal variable values exists at the extremes of the variable ranges in all but one variable (A). m^K variable sampling chooses design points incorporating the optimal values, while NOBLH does not.

Had the models required more computational rigor (more factors or computations) the NOBLH samplings' efficiency might have provided insights into optimization where m^k factorial design would have been too costly. However, with both our three- and six-variable models we do not have difficulty evaluating m^k factorial samplings even with double digit levels (m).

6.1.4 Iterative Method

The NOBLH iterative methods we use for the three- and six-variable models are ad hoc methods that arose from trying to glean more insight about our models' behavior. Had we been interested solely in identifying an optimal solution, then an adaptive sequential procedure, such as response surface methodology [34], STRONG [35], or other simulation optimization approaches would require much less sampling.

6.1.5 Robustness Analysis

After determining the optimal variable values, our analysis turns to evaluating the robustness of the variables by evaluating power generation while incorporating deviations from

the optimal variable values. In the three-variable model, we find the separation between the frequency of excitation of the base (ω) and natural frequency of the generator (ω_n) to be the most sensitive variable. While the designers of the piezoelectric generator should seek to minimize the generator's modal damping ratio (ζ), the designer's priority should be to precisely match the generator's natural frequency with the frequency of excitation driving the generator.

The precise matching of the base motion driving frequency (ω_{base}) to the modal short circuit net frequency (w_{SC}) proves to be the most important factor in minimizing power loss during the robustness analysis of the six-variable model. Setting the electromagnetic coupling coefficient (A), load resistance (R), and net clamped capacity of piezoelectric material (C_0) to their respective optimal value is a much lower priority for the piezoelectric generator designer. In fact, our robustness study concludes if the likelihood of negative variation is greater than or equal to positive variation for the design's modal damping ratio, it is best to let ζ vary from its optimal value while restraining the variation of other variables from their optimal values in order to produce the greatest mean power output.

6.2 Further Studies

Through the analysis of two mathematical models, we determine optimal values for each variable, given a practical variable range in order to maximize power generation of a piezoelectric generator. Additional studies are needed to propel our findings into practical application of piezoelectric materials for energy harvesting.

6.2.1 PDE Solution

To derive the nine variable model in Chapter 3, we use a one-mode expansion method. An alternative methods to derive models would be to use a partial differential equation expansion [36]. This mathematical derivation would provide an additional piezoelectrical generator model to conduct further optimization studies.

6.2.2 Variable Range Adjustment

We derive the variable ranges through research of materials specifications and previous experimental measurements. Personnel more experienced in vibration, piezoelectric materials, and electrical engineering will have the ability to further adjust the ranges for each

variable. Using our methods of analysis and power generation models, it is possible to find updated optimal values for each variable.

6.2.3 Simulation Optimization

In future studies, an automated simulation optimization technique would be a better approach for finding optimal nominal settings for the variables while keeping sampling requirements to a minimum.

6.2.4 Robustness Analysis Expansion

Our efforts study the robustness of the two power generation models based on both single and multiple variable manipulation. In both the three- and six-variable power manipulation, we assume the environment to be static. In other words, we assume the frequency of excitation (ω) and the base motion driving frequency to be constant for the three- and six-variable models, respectively. This enables us to focus our robustness study on fewer variables.

In practical applications, the frequency of the driving vibration may not prove constant. The vibration of an air conditioning duct may change based on temperature, humidity, fan speed, or a myriad other factors. Further robustness analysis focused on the base motion driving frequency may lead to a better piezoelectric generator power output in varying environmental conditions.

6.2.5 Model Adjustment

The two mathematical models we use do not serve as the only models to simulate piezoelectric power production. Further studies could include additional models or adjustments to the two models used in this study. The optimization and robustness analysis methodologies in this study could serve as a framework in the study of new models.

6.2.6 Practical Experimentation

We gear the efforts of this paper in order to find insights into maximizing piezoelectric generator power output. Using our findings, engineers can attempt to match our modeled results using a prototype piezoelectric generator designed with our optimal variable values. Feedback from the results of the experimentation could serve to adjust our models or variable limits.

APPENDIX: MATLAB Codes

A.1 Three-Variable Orthogonality Computation Code

```
%3 Variable Orthogonality Computation
%Created April 2015 by Russell Nelson

clear all

%Import design points
filename = 'Factorial3var.csv';

%Rename file
NOLH=csvread(filename);

%Compute orthogonality for each variable
avgomega = mean(NOLH(:,1));
avgomega_n = mean(NOLH(:,2));
avgzeta = mean(NOLH(:,3));
numerator1 = 0;
numerator2 = 0;
numerator3 = 0;
denom11 = 0;
denom12 = 0;
denom21 = 0;
denom22 = 0;
denom31 = 0;
denom32 = 0;
for i = 1:1000
    omegai = NOLH(i,1);
    omega_ni = NOLH(i,2);
    numerator1 = numerator1 + (omegai-avgomega)*(omega_ni-avgomega_n);
    denom11 = denom11 + (omegai-avgomega)^2;
    denom12 = denom12 + (omega_ni-avgomega_n)^2;
end
%Outputs correlation for omega to omega_n
Ortho_omega_omega_n=numerator1/sqrt(denom11*denom12)
```

```
for i = 1:1000
    omegai = NOLH(i,1);
    zetai = NOLH(i,3);
    numerator2 = numerator2 + (omegai-avgomega)*(zetai-avgzeta);
    denom21 = denom21 + (omegai-avgomega)^2;
    denom22 = denom22 + (zetai-avgzeta)^2;
end
%Outputs correlation for omega to zeta
Ortho_omega_zeta = numerator2/sqrt(denom21*denom22)

for i = 1:1000
    omega_ni = NOLH(i,2);
    zetai = NOLH(i,3);
    numerator3 = numerator3 + (omega_ni-avgomega_n)*(zetai-avgzeta);
    denom31 = denom31 + (omega_ni-avgomega_n)^2;
    denom32 = denom32 + (zetai-avgzeta)^2;
end
%Outputs correlation for omega_n to zeta
Ortho_omega_n_zeta = numerator3/sqrt(denom31*denom32)
```

A.2 Six-Variable Orthogonality Computation Code

```
%6 Variable Orthogonality Computation
%Created April 2015 by Russell Nelson

clear all

%Import design points
filename = 'Factorial6var.csv';

%Rename file
NOLH=csvread(filename);

%Compute orthogonality for each variable
num=0;
den1=0;
den2=0;
```

```
for d = 2:6
    for i =1:15625
        Ai = NOLH(i,1);
        Bi = NOLH(i,d);
        avA = mean(NOLH(:,1));
        avB = mean(NOLH(:,d));
        num = num + (Ai-avA)*(Bi-avB);
        den1 = den1 +(Ai-avA)^2;
        den2 = den2 +(Bi-avB)^2;
    end
   OrthoA(d)= num/sqrt(den1*den2);
end

num=0;
den1=0;
den2=0;
for d = 3:6
    for i =1:15625
        Ai = NOLH(i,2);
        Bi = NOLH(i,d);
        avA = mean(NOLH(:,2));
        avB = mean(NOLH(:,d));
        num = num + (Ai-avA)*(Bi-avB);
        den1 = den1 +(Ai-avA)^2;
        den2 = den2 +(Bi-avB)^2;
    end
   OrthoR(d)= num/sqrt(den1*den2);
end

num=0;
den1=0;
den2=0;
for d = 4:6
    for i =1:15625
        Ai = NOLH(i,3);
        Bi = NOLH(i,d);
        avA = mean(NOLH(:,3));
        avB = mean(NOLH(:,d));
        num = num + (Ai-avA)*(Bi-avB);
```

```
        den1 = den1 +(Ai-avA)^2;
        den2 = den2 +(Bi-avB)^2;
    end
   OrthoO(d)= num/sqrt(den1*den2);
end

num=0;
den1=0;
den2=0;
for d = 5:6
    for i =1:15625
        Ai = NOLH(i,4);
        Bi = NOLH(i,d);
        avA = mean(NOLH(:,4));
        avB = mean(NOLH(:,d));
        num = num + (Ai-avA)*(Bi-avB);
        den1 = den1 +(Ai-avA)^2;
        den2 = den2 +(Bi-avB)^2;
    end
   OrthoC(d)= num/sqrt(den1*den2);
end

num=0;
den1=0;
den2=0;
for d = 6:6
    for i =1:15625
        Ai = NOLH(i,5);
        Bi = NOLH(i,d);
        avA = mean(NOLH(:,5));
        avB = mean(NOLH(:,d));
        num = num + (Ai-avA)*(Bi-avB);
        den1 = den1 +(Ai-avA)^2;
        den2 = den2 +(Bi-avB)^2;
    end
   OrthoW(d)= num/sqrt(den1*den2);
end
```

A.3 Euclidean Maximin Distance Code

```
%Euclidean Maximin Distance Calculator
%Created April 2015 by Russell Nelson
clear all

%Import factorial design points to use
%as reference
file = 'Factorial3var.csv';
base = csvread(file);

%Import Design Points
filename = 'Factorial3var.csv';

%Rename file
A=csvread(filename);

%Establish number of variables (n)
%and number of design points (k)
[n,k] = size(NOLH);
d=0;
i=1;

%Normalizing vectors
for p = 1:k
    avg = (max(base(:,p))-min(base(:,p)))/2+min(base(:,p));
    for q = 1:n
        A(q,p) = (A(q,p)-avg)/avg;
    end
end

%Computing all distances
for s = 1:n
    for t = 2:n
        if s == t
        else
            for j = 1:k
            d = d + abs(A(s,j)-A(t,j))^2;
```

```
            end
            d = sqrt(d);
            distance(i) = d;
            d=0;
            i = i+1;
        end
    end
end

%Finding the Euclidean maximin distance
min(distance)
```

A.4 Three-Variable Model Optimization Code for Factorial Sampling

```
%Optimal Power for Three Variable Model (Factorial Sampling Method)
%Created January 2015 by Russell Nelson.

%The following script evaluates the average power dissipated by the load
%resistor of a piezoelectric generator.  The equation, consisting of 3
%independent variables, was derived by Professor Hong Zhou.
clear all

a=1;
b=1;
c=1;

%Set variable limits (range)
omega_min_lim = 120*pi;
omega_max_lim = 360*pi;
omega_n_min_lim = 120*pi;
omega_n_max_lim = 360*pi;
zeta_min_lim = 0.005;
zeta_max_lim = 0.02;

%Set number of levels per variables
levels = 100;
```

```
%Computes values of power for all combinations of
%variables at all levels
for omega = linspace(omega_min_lim,omega_max_lim,levels)
    b=1;
    for omega_n = linspace(omega_n_min_lim,omega_n_max_lim,levels)
        c=1;
       for zeta = linspace(zeta_min_lim,zeta_max_lim,levels)
           P(a,b,c) = (zeta*((omega/omega_n)^3)*(omega^3))/...
           ((1-((omega^2)/(omega_n^2)))^2+...
           (2*zeta*(omega/omega_n))^2);
           c=c+1;
       end
       b=b+1;
    end
    a=a+1;
end

%Vectorizes P matrix
Pvec=P(:);

%Find the maximum power in Pvec
[v,I]=max(Pvec)

%Determines the location of each variable level for maximum power
[d,e,f]=ind2sub(size(P),I);

%Determines the value for each variable at maximum power
omega = linspace(omega_min_lim,omega_max_lim,levels);
omegaopt=omega(d)
omega_n = linspace(omega_n_min_lim,omega_n_max_lim,levels);
omega_nopt=omega_n(e)
zeta = linspace(zeta_min_lim,zeta_max_lim,levels);
zetaopt=zeta(f)
```

A.5 Three-Variable Model Optimization Code for NOBLH Sampling

```
%3 Variable Model Optimization Code for NOBLH Sampling
%Created January 2015 by Russell Nelson

%The following script evaluates the average power dissipated by the load
%resistor of a piezoelectric generator.  The equation, consisting of 3
%independent variables, was derived by Professor Hong Zhou.

clear all

%Import design points
filename = 'NOL3var.csv';

%Rename file
NOLH=csvread(filename);

%Compute power for all design points
for i =1:512
    omega=NOLH(i,1);
    omega_n=NOLH(i,2);
    zeta=NOLH(i,3);
    Power(1,i) = (zeta*((omega/omega_n)^3)*(omega^3))/...
    ((1-((omega^2)/(omega_n^2)))^2+(2*zeta*(omega/omega_n))^2);
end

%Identify maximum power and associated design point
[x,y]=max(Power)
```

A.6 Six-Variable Model Optimization Code for Factorial Sampling

```
%Optimal Power for Six Variable Model (Factorial Sampling Method)
%Created January 2015 by Russell Nelson

%The following script evaluates the average power dissipated by the load
%resistor of a piezoelectric generator.  The equation, consisting of 6
%independent variables, used was derived by Professor Hong Zhou.
```

```
clear all

a=1
b=1;
c=1;
d=1;
e=1;
f=1;

%Set variable limits(range)
A_min_lim = 0.01;
A_max_lim = 0.99;
R_min_lim = .02;
R_max_lim = 100;
Obase_min_lim = 120*pi;
Obase_max_lim = 360*pi;
C0_min_lim = 0.00000001;
C0_max_lim = 0.000001;
WSC_min_lim = 120*pi;
WSC_max_lim = 360*pi;
zeta_min_lim = 0.005;
zeta_max_lim = 0.02;
%Set number of levels per variable
levels=12;

%Computes values of power for all combinations of
%variables at all levels
for A = linspace(A_min_lim,A_max_lim,levels)
 b=1;
 for R = linspace(R_min_lim,R_max_lim,levels)
  c=1;
  for Obase = linspace(Obase_min_lim,Obase_max_lim,levels)
   d=1;
   for C0 = linspace(C0_min_lim,C0_max_lim,levels)
    e=1;
    for WSC = linspace(WSC_min_lim,WSC_max_lim,levels)
     f=1;
     for zeta = linspace(zeta_min_lim,zeta_max_lim,levels)
```

```
      P(a,b,c,d,e,f) =(A^2*R*Obase^6*(1+C0^2*Obase^2*R^2)^2)/...
      (2*(((-1*Obase^2+WSC^2)*(1+C0^2*Obase^2*R^2)+(C0*A^2)*...
      Obase^2*R^2)^2+(2*WSC*zeta*Obase*(1+C0^2*Obase^2*R^2)...
      +A^2*Obase*R)^2));
      f=f+1;
     end
     e=e+1;
    end
    d=d+1;
   end
   c=c+1;
  end
  b=b+1;
 end
 a=a+1;
end

%Vectorizes P matrix
Pvec=P(:);
%Finds the maximum power in Pvec
[v,I] = max(Pvec)
%Determines the location of each variable level for maximum power
[j,k,l,m,n,o]=ind2sub(size(P),I);
%Determines the value for each variable at maximum power
A = linspace(A_min_lim,A_max_lim,levels);
Aopt = A(j)
R = linspace(R_min_lim,R_max_lim,levels);
Ropt = R(k)
Obase = linspace(Obase_min_lim,Obase_max_lim,levels);
Obaseopt = Obase(l)
C0 = linspace(C0_min_lim,C0_max_lim,levels);
C0opt = C0(m)
WSC = linspace(WSC_min_lim,WSC_max_lim,levels);
WSCopt = WSC(n)
zeta = linspace(zeta_min_lim,zeta_max_lim,levels);
zetaopt = zeta(o)
```

A.7 Six-Variable Model Optimization Code for NOBLH Sampling

```
%6 Variable Model Optimization Code for NOBLH Sampling
%Created January 2015 by Russell Nelson

%The following script evaluates the average power dissipated by the load
%resistor of a piezoelectric generator.  The equation, consisting of 6
%independent variables, used was derived by Professor Hong Zhou.

clear all

%Import design points
filename = 'NOL6var.csv';

%Rename file
NOLH=csvread(filename);

%Compute power for all design points
for i =1:512
    A=NOLH(i,1);
    R=NOLH(i,2);
    Obase=NOLH(i,3);
    C0=NOLH(i,4);
    WSC=NOLH(i,5);
    zeta=NOLH(i,6);
    Power(1,i) =(A^2*R*Obase^6*(1+C0^2*Obase^2*R^2)^2)/...
      (2*(((-1*Obase^2+WSC^2)*(1+C0^2*Obase^2*R^2)+(C0*A^2)*...
      Obase^2*R^2)^2+(2*WSC*zeta*Obase*(1+C0^2*Obase^2*R^2)...
      +A^2*Obase*R)^2));
end

%Identify maximum power and associated design point
[x,y]=max(Power)
```

THIS PAGE INTENTIONALLY LEFT BLANK

List of References

[1] E. Rosenthal. (2010, Oct. 4). US military orders less dependence on fossil fuels. *New York Times* [Online]. Available: http://www.nytimes.com/2010/10/05/science/earth/05fossil.html.

[2] S. Hargreaves. (2011, Aug. 17). For the military clean fuel saves lives. [Online]. Available: http://money.cnn.com/2011/08/17/technology/militaryenergy/.

[3] A. Manbachi and R. S. Cobbold, "Development and application of piezoelectric materials for ultrasound generation and detection," *Ultrasound*, vol. 19, no. 4, pp. 187–196, 2011.

[4] Quartz clock. (2015). *Wikipedia*. Available: http//en.wikipedia.org/wiki/Quartzclock. Accessed Apr. 15, 2015.

[5] A. Arnau Vives, *Piezoelectric transducers and applications*. Berlin, Germany: Springer, 2008.

[6] W. P. Mason, "Piezoelectricity, its history and applications," *The Journal of the Acoustical Society of America*, vol. 70, no. 6, pp. 1561–1566, 1981.

[7] G. Akhras and W. Li, "Three-dimensional static, vibration and stability analysis of piezoelectric composite plates using a finite layer method," *Smart materials and structures*, vol. 16, no. 3, p. 561, 2007.

[8] H. Bai, A. Shah, S. Dong, and E. Taciroglu, "End reflections in a layered piezoelectric circular cylinder," *International Journal of Solids and Structures*, vol. 43, no. 20, pp. 6309–6325, 2006.

[9] X. Liu, Q. Wang, and S. Quek, "Analytical solution for free vibration of piezoelectric coupled moderately thick circular plates," *International Journal of Solids and Structures*, vol. 39, no. 8, pp. 2129–2151, 2002.

[10] G. Qing, J. Qiu, and Y. Liu, "A semi-analytical solution for static and dynamic analysis of plates with piezoelectric patches," *International Journal of Solids and Structures*, vol. 43, no. 6, pp. 1388–1403, 2006.

[11] B.-G. Nam and K. Watanabe, "Crack energy density and energy release rate for piezoelectric material," *International Journal of Solids and Structures*, vol. 44, no. 11, pp. 3904–3919, 2007.

[12] A. Benjeddou and J.-F. Deü, "A two-dimensional closed-form solution for the free-vibrations analysis of piezoelectric sandwich plates," *International Journal of Solids and Structures*, vol. 39, no. 6, pp. 1463–1486, 2002.

[13] D. A. Saravanos, P. R. Heyliger, and D. A. Hopkins, "Layerwise mechanics and finite element for the dynamic analysis of piezoelectric composite plates," *International Journal of Solids and Structures*, vol. 34, no. 3, pp. 359–378, 1997.

[14] Y. Liao and H. A. Sodano, "Model of a single mode energy harvester and properties for optimal power generation," *Smart Materials and Structures*, vol. 17, no. 6, p. 065026, 2008.

[15] S. Roundy and P. K. Wright, "A piezoelectric vibration based generator for wireless electronics," *Smart Materials and Structures*, vol. 13, no. 5, p. 1131, 2004.

[16] N. E. Dutoit, B. L. Wardle, and S.-G. Kim, "Design considerations for mems-scale piezoelectric mechanical vibration energy harvesters," *Integrated Ferroelectrics*, vol. 71, no. 1, pp. 121–160, 2005.

[17] C. Williams and R. B. Yates, "Analysis of a micro-electric generator for microsystems," *Sensors and Actuators A: Physical*, vol. 52, no. 1, pp. 8–11, 1996.

[18] S. R. Anton and H. A. Sodano, "A review of power harvesting using piezoelectric materials (2003–2006)," *Smart Materials and Structures*, vol. 16, no. 3, p. R1, 2007.

[19] A. M. Wickenheiser and E. Garcia, "Power optimization of vibration energy harvesters utilizing passive and active circuits," *Journal of Intelligent Material Systems and Structures*, vol. 21, no. 13, pp. 1343–1361, 2010.

[20] J. Scruggs, "An optimal stochastic control theory for distributed energy harvesting networks," *Journal of Sound and Vibration*, vol. 320, no. 4, pp. 707–725, 2009.

[21] N. W. Hagood, W. H. Chung, and A. Von Flotow, "Modelling of piezoelectric actuator dynamics for active structural control," *Journal of Intelligent Material Systems and Structures*, vol. 1, no. 3, pp. 327–354, 1990.

[22] H. A. Sodano, G. Park, and D. Inman, "Estimation of electric charge output for piezoelectric energy harvesting," *Strain*, vol. 40, no. 2, pp. 49–58, 2004.

[23] H. T. Banks and D. Inman, "On damping mechanisms in beams," *Journal of Applied Mechanics*, vol. 58, no. 3, pp. 716–723, 1991.

[24] A. Fleming, S. Behrens, and S. Moheimani, "Reducing the inductance requirements of piezoelectric shunt damping systems," *Smart Materials and Structures*, vol. 12, no. 1, p. 57, 2003.

[25] S. M. Sanchez and H. Wan, "Work smarter, not harder: A tutorial on designing and conducting simulation experiments," in *Proceedings of the 2012 Winter Simulation Conference*, C. Laroque, J. Himmelspach, R. Pasupathy, O. Rose, and A. Uhrmacher, Eds. Piscataway, NJ: Institute of Electrical and Electronic Engineers, Inc., 2012, pp. 1929–1943.

[26] K. Q. Ye, "Orthogonal column Latin hypercubes and their application in computer experiments," *Journal of the American Statistical Association*, vol. 93, no. 444, pp. 1430–1439, 1998.

[27] T. M. Cioppa, "Efficient nearly orthogonal and space-filling experimental design for high-dimensional complex models," Ph.D. dissertation, Naval Postgraduate School, Monterey, CA, 2002.

[28] T. M. Cioppa and T. W. Lucas, "Efficient nearly orthogonal and space-filling Latin hypercubes," *Technometrics*, vol. 49, no. 1, 2007.

[29] H. Vieira Jr., S. Sanchez, K. Kienitz, and M. Belderrain, "Improved efficient, nearly orthogonal, nearly balanced mixed designs," in *Proceedings of the 2011 Winter Simulation Conference*, S. Jain, R. Creasey, J. Himmelspach, K. White, and M. Fu, Eds. Phoenix, AZ: Institute of Electrical and Electronic Engineers, Inc., 2011, pp. 3605–3616.

[30] H. Vieira Jr., "Nob mixed 512dp template v1.xls design spreadsheet," http//harvest.edu/, 2012, accessed Mar, 24th 2015.

[31] V. R. Joseph and Y. Hung, "Orthogonal-maximin Latin hypercube designs," *Statistica Sinica*, vol. 18, no. 1, p. 171, 2008.

[32] S. M. Sanchez, "Robust design: Seeking the best of all possible worlds," in *Proceedings of the 2000 Winter Simulation Conference*, J. A. Joines, R. R. Barton, K. Kang, and P. A. Fishwick, Eds. Piscataway, NJ: Institute of Electrical and Electronic Engineers, Inc., 2000, pp. 69–76.

[33] P. Tucker. (2015, May 5). Here's what the new tesla battery means for the military. [Online]. Available: http://www.defenseone.com/technology/2015/05/heres-what-new-tesla-battery-means-national-security/111928/.

[34] R. H. Myers, D. C. Montgomery, and C. M. Anderson-Cook, *Response Surface Methodology*, 3rd ed. New York: Wiley, 2009.

[35] K. Chang, J. L. Hong, and H. Wan, "Stochastic trust region gradient-free method (STRONG)–a new response-surface-based algorithm in simulation optimization," *INFORMS Journal on Computing*, vol. 25, no. 2, pp. 230–243, 2013.

[36] M. Abu-Hilal, “Forced vibration of euler–bernoulli beams by means of dynamic green functions,” *Journal of Sound and Vibration*, vol. 267, no. 2, pp. 191–207, 2003.

Initial Distribution List

1. Defense Technical Information Center
   Ft. Belvoir, Virginia

2. Dudley Knox Library
   Naval Postgraduate School
   Monterey, California